Taflanidis AA, Giaralis A and Patsialis D (2019) Multi-objective optimal design of inerter-based vibration absorbers for earthquake protection of multi-storey building structures. *Journal of the Franklin Institute, accepted* (13/02/2019)

Multi-objective optimal design of inerter-based vibration absorbers for earthquake protection of multi-storey building structures

A.A. Taflanidis[a], A. Giaralis[b*] and D. Patsialis[a]

[a]*Department of Civil & Environmental Engineering & Earth Sciences, University of Notre Dame, Notre Dame, IN 46556, USA*
[b]*Department of Civil Engineering, City, University of London, EC1V 0HB, London, UK*

Abstract

In recent years different inerter-based vibration absorbers (IVAs) emerged for the earthquake protection of building structures coupling viscous and tuned-mass dampers with an inerter device. In the three most popular IVAs the inerter is functioning either as a motion amplifier [tuned-viscous-mass-damper (TVMD) configuration], mass amplifier [tuned-mass-damper-inerter (TMDI) configuration], or mass substitute [tuned-inerter-damper (TID) configuration]. Previous work has shown that through proper tuning, IVAs achieve enhanced earthquake-induced vibration suppression and/or weight reduction compared to conventional dampers/absorbers, but at the expense of increased control forces exerted from the IVA to the host building structure. These potentially large forces are typically not accounted for by current IVA tuning approaches. In this regard, a multi-objective IVA design approach is herein developed to identify the compromise between the competing objectives of (i) suppressing earthquake-induced vibrations in buildings, and (ii) avoiding development of excessive IVA (control) forces, while, simultaneously, assessing the appropriateness of different modeling assumptions for practical design of IVAs for earthquake engineering applications. The potential of the approach to pinpoint Pareto optimal IVA designs against the above objectives is illustrated for different IVA placements along the height of a benchmark 9-storey steel frame structure. Objective (i) is quantified according to current performance-based seismic design trends using first-passage reliability criteria associated with the probability of exceeding pre-specified thresholds of storey drifts and/or floor accelerations being the engineering demand parameters (EDPs) of interest. A variant, simpler, formulation is also considered using as performance quantification the sum of EDPs variances in accordance to traditional tuning methods for dynamic vibration absorbers. Objective (ii) is quantified through the variance of the IVA force. It is found that reduction of IVA control force of up to 3 times can be achieved with insignificant deterioration of building performance compared to the extreme Pareto optimal IVA design targeting maximum vibration suppression, while TID and TMDI achieve practically the same building performance and significantly outperform the TVMD. Moreover, it is shown that the simpler variant formulation may provide significantly suboptimal reliability performance. Lastly, it is verified that the efficacy of optimal IVA designs for stationary conditions is maintained for non-stationary stochastic excitation model capturing typical evolutionary features of earthquake excitations.

Keywords: Inerter-based vibration suppression; seismic protection; multi-objective design; first-passage reliability; stationary response; peak inerter force

* Corresponding author. Senior Lecturer, Department of Civil Engineering, City University London, London, UK. Email: Agathoklis.Giaralis.1@city.ac.uk

1. Introduction

Earthquake resistant design of building structures for reduced upfront cost is regularly addressed through ductile behavior of their lateral load resisting system, involving dissipation of the input seismic (kinetic) energy through inelastic (hysteretic) behavior (see e.g, [1] and references therein). Nevertheless, this seismic design strategy may incur significant structural damages, yielding excessive repair cost and downtime in the aftermath of severe earthquake events. To this end, considerable research for development and application of passive viscous and viscoelastic dampers endowing supplemental damping to building structures has been undertaken over the past three decades to minimize seismic losses, achieving, ideally, linear structural response during major earthquake events [2]. To this aim, these dampers, coupled with stiffeners and connectors, are placed in between building floors [3], hence, acting as diagonal struts engaged by the relative lateral motion of building slabs under seismic excitation. Alternatively, they are used in tuned mass dampers (TMDs) to connect a pre-specified secondary free-to-oscillate mass (close) to the top floor, tuned to counteract the building motion [4]. Stiffness and damping properties of both the above passive vibration control configurations are designed/tuned to enhance the *seismic performance* of the uncontrolled (host) building structure by mitigating critical to seismic loss earthquake response quantities, termed engineering demand parameters (EDPs) in modern performance-based earthquake engineering [5], such as relative displacement between building floors, henceforth storey drifts, and absolute floor accelerations.

In this setting, recently, different linear passive *inerter-based vibration absorbers* (IVAs) emerged [6-17] achieving improved seismic building performance and/or secondary attached mass reduction by incorporating an *inerter* to conventional energy dissipating diagonal struts and TMDs. The inerter has been theoretically defined by Smith [18], aiming to facilitate passive network synthesis approaches for general vibration control applications, as a linear massless two-terminal mechanical element resisting relative acceleration by a force proportional to a constant termed *inertance* and measured in mass units (kg). Moreover, in [18], the feasibility to materialize an inerter device whose inertance scales up practically independently of its weight has been established by considering mechanisms transforming, through gearing, the translational motion of the device terminals into rotational motion of a flywheel (i.e., a lightweight fast-spinning disk) [19, 20]. Lately, alternative fluid-based inerter devices (e.g., [21, 22]) as well as inertance emulation in the electrical domain using electromagnetic motors (e.g., [23, 24]) have further been developed. Nevertheless, prior to and independently of the above works, the viscous mass damper (VMD) introduced by Arakaki et al. [25], also termed as rotational damper or gyro-damper [26], was historically one of the first vibration control devices for earthquake engineering applications to incorporate a ball-screw inerter-like mechanism. Specifically, in the VMD, the ball-screw mechanism acts as a *motion amplifier* to increase seismic energy dissipation in a viscous damper by transforming relatively slow translational

motion (e.g., between two floors of a building connected through a VMD diagonal strut) to fast rotational motion of a circular drum placed in viscous (solid or fluid) material [14]. In this regard, the VMD device can be viewed as an IVA represented by an inerter in parallel with a dashpot [26]. In later years, a flywheel was incorporated to the VMD for increased inertance and a spring tuned to a particular (targeted) mode of the host building structure was added in series with the VMD giving birth to the *tuned viscous-mass-damper* (TVMD) [7, 13]. The latter is the first IVA to have been implemented in actual structures in Japan [27]. More recently, two different IVAs have been independently proposed, namely the tuned mass-damper-inerter (TMDI) [9, 17] and the tuned inerter-damper (TID) [6], utilizing the inerter as a weightless mass element to improve the efficiency of TMDs for seismic protection of buildings while relaxing, for the TMDI, or eliminating, for the TID, requirements for excessive secondary TMD mass typically necessitated in earthquake engineering applications (see e.g., [28] and references therein). Specifically, in the TMDI, the inerter acts as a *mass amplifier* contributing inertia (but not weight) to a conventional TMD by connecting the secondary mass to a different floor from the one that the TMD is attached to. While in the TID, the inerter is used as a *surrogate* of the TMD secondary mass resulting in a diagonal strut comprising a viscoelastic damper (spring in parallel to dashpot) in series with an inerter connecting two adjacent floors. Alternative IVAs comprising more than three (i.e., a single spring, damper, and inerter) elements have been pursued lately for further seismic building performance improvement relying on passive network synthesis approaches [11, 12]. Once an optimal IVA configuration is reached for a particular host structure through these approaches, less complex diagonal struts (e.g., TID, TVMD or some variants) favoring practical implementation may be sought after by establishing similar seismic performance (to the identified optimal configuration) within a frequency band of interest [17].

Irrespective of their complexity and layout, optimal design of the aforementioned IVAs has been frequently addressed by relying on traditional tuning approaches to a particular host structure natural frequency widely applicable to mass dampers, such as the "fixed-point tuning" in [29], aiming to suppress the peak of the frequency response function (FRF) of the host structure [6, 7, 11, 30]. Shortcomings of such $\mathcal{H}_\infty$ style optimal design approaches are that (I) seismic excitation frequency content and, therefore, structural response, is broadband and uncertain in nature deviating significantly from single harmonic conditions [31] implied by $\mathcal{H}_\infty$ optimization, and (II), contrary to traditional mass dampers, IVAs have been shown to impact dynamic behaviour of the host structure in a wide frequency range, beyond the specific frequency they are tuned at [32-34]. The above shortcomings incentivized several researchers to pursue optimal IVA design against stationary stochastic structural performance metrics modelling dynamic (seismic) excitation as white noise [35-37] or, more appropriately (see e.g., [31]), as colored noise [12, 17, 32]. Indeed, adopting a stochastic description of the performance facilitates a more faithful description of seismic excitation while it explicitly considers the ability of IVAs for wideband vibration suppression, as

stochastic response is evaluated considering contribution from all frequencies [31] leading to an $\mathcal{H}_2$ style of optimality. This ability can further be exploited, if deemed necessary, by considering floor accelerations as EDPs which are more sensitive to higher-order vibration modes in multi-storey buildings and associated with seismic loss due to failures (e.g., sliding and/or toppling) of sensitive equipment, furniture, and artefacts housed in buildings. Meanwhile, representing the seismic input action by a stochastic process circumvents the need to design for any particular (recorded) ground motion, as for example considered in [38], which does not necessarily facilitate optimal seismic performance to future seismic excitations due to the natural uncertainty of earthquake ground motions.

Independently of the design approach, seismic performance enhancement offered by IVAs comes at the expense of increased (control) forces developed within the IVA and transferred to the host structure [15, 27, 33, 36, 39]. Such large forces govern the upfront cost of inerters and dampers. Further, they need to be accommodated by the host structure, potentially through local strengthening of structural members (i.e., columns, beams and braces) supporting the IVA, a feature that is becoming increasingly a concern in applications of control devices to typical medium- and high-rise building structures [40]. In this regard, this paper examines the multi-objective design of IVAs, focusing on the three most widely considered in the literature IVAs, that is the TVMD, TMDI, and TID, for seismic risk mitigation of building structures aiming to quantify in a practical context the compromise between the competing objectives of improving seismic performance and avoiding large IVA control forces. For formulating the design problem, fixed configurations of dashpot, spring and inertia (inerter and mass for the case of the TMDI) elements is assumed and optimal properties of all elements within a practically meaningful search range are identified for a given host structure. Seismic excitation is modeled as stationary colored stochastic process and structural behavior through a linear dynamical system, utilizing a state-space formulation. Two different formulations are used to define the first objective, representing the seismic building performance. The main formulation uses first-passage reliability criteria associated with the probability that the adopted EDPs (i.e., storey drifts and/or floor accelerations) overshoot prescribed design-specific thresholds. An alternative, simpler, formulation uses the sum of variances of the adopted EDPs. Note that the former reliability-based seismic performance quantification has previously been considered only in [32] for single-objective optimal design of TMDI, and is better aligned with objectives set by current performance-based structural engineering standards [26, 27] compared to stationary response variances considered by the rest of the above reviewed works for $\mathcal{H}_2$ style optimal IVA design. Herein, optimal designs derived from the two different formulations are compared. The second objective, representing the upfront IVA cost as well as local strengthening of the host structure, corresponds to the stationary force transferred by the IVA to the structure. Beyond the multi-objective design, in this work the achieved performance of dual-objective optimal IVA designs under stationary excitation is also assessed under non-stationary in amplitude colored

stochastic seismic excitation using appropriately defined metrics corresponding to the two objectives adopted in design. This assessment serves as a validation of the assumption of stationary conditions at the design stage, by performing a comparison of the performance under stationary and non-stationary excitation conditions.

The major contribution of the present study is that it offers a comprehensive mapping of the trade-off between the competing objectives of vibration suppression and peak developing control force under optimal IVA design, adopting seismic performance quantification metrics and excitation model tailored for the application at hand. This is also accomplished by furnishing numerical results in the form of optimal Pareto design solutions for a 9-storey benchmark steel frame building structure purpose-developed for assessing vibration control solutions in earthquake engineering [41], as opposed to simpler examples of ideal, shear-type frame buildings adopted in works found in the literature addressing optimal IVA design. In this respect, it is parenthetically noted that Pan et al. [36] also examined multi-objective optimization of a TVMD-variant. Their study was constrained, though, to a single IVA type, a single-storey host structure, a simplified description of the excitation (white noise) and of the performance (response variance), while it did not present a comprehensive evaluation of the Pareto optimality established by considering the compromise between the competing objectives. Note that the latter is essential for facilitating decisions within a multi-criteria design setting [42]. Other novel contributions of the present work include the comparison of optimal IVA designs achieved using reliability-based criteria vis-à-vis EDP variances for seismic performance quantification, as well as the validation of the assumption of stationary conditions at the design stage vis-à-vis non-stationary amplitude-dependent excitation conditions.

In the remainder of the paper, the governing equations of motion of the dynamical system in state-space are presented in the next section, followed (Section 3) by the stationary response statistics calculation and (Section 4) by the multi-objective design problem formulation. Section 5 furnishes pertinent numerical data of optimal IVA designs and performance for the case-study benchmark building structure exposed to stationary stochastic seismic excitation, while Section 6 verifies these designs against non-stationary seismic excitation within a Monte Carlo-based context. Concluding remarks are summarized in Section 7.

2. Equations of motion of multi-storey structures equipped with inerter-based vibration absorbers

Consider the planar *n*-storey frame building, shown in Figure 1, whose oscillatory motion due to a ground acceleration $\ddot{x}_g$ is to be suppressed hosting an IVA. As discussed in the introduction different IVAs can be established by combining an inerter with springs (stiffness elements), dashpots (damper elements) and, even, secondary masses in series and/or parallel connectivity. In this regard, a generic 5-element IVA is

herein considered connecting two not necessarily consecutive floors, i_d and i_b, and comprising an intermediate (secondary) mass, m_d, attached to the upper i_d floor via a viscoelastic link (linear spring and dashpot in parallel) and to the lower i_b floor via a VMD (dashpot in parallel with inerter) as shown in Figure 1. By judicially eliminating one or more elements (i.e., setting to zero certain properties), the considered generic IVA enables modelling the three most-widely studied IVAs discussed in the introduction, namely the TVMD, the TMDI and the TID, as indicated in the inlets of Figure 1. Since TVMD and TID are mostly used as diagonal struts, practical and architectural configurations require that they connect adjacent floors, i.e., i_b-i_d=1. Nevertheless, the TMDI may observe i_b-i_d>1 as practical [32], with the secondary mass allowing implementations that span multiple floors as in the commonly considered in practice case of pendulum-like TMDs [4].

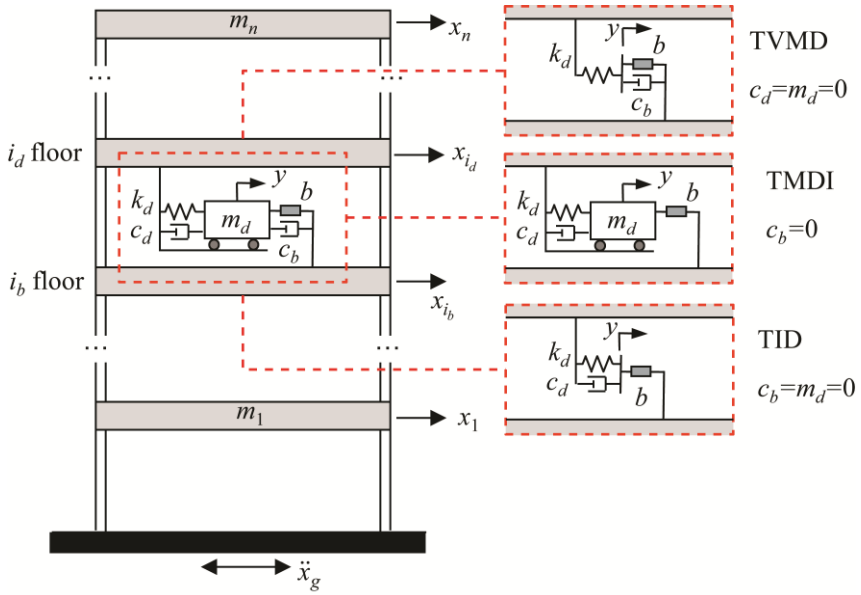

Figure 1: Multi-storey structure equipped with different inerter-based vibration absorbers.

Let $\mathbf{x}_s \in \Re^n$ be the vector of floor displacements of the host structure relative to the ground and $\ddot{x}_g \in \Re$ be the ground acceleration. Denote by $\mathbf{R}_d \in \Re^n$ the *spring location* vector specifying the floor the spring (along with potential dashpot) is attached to, that is vector of zeros with a single one in its i_d entry, and by $\mathbf{R}_b \in \Re^n$ the *inerter location* vector specifying the floor the inerter (along with potential dashpot) is connected to, that is vector of zeros with a single one in its i_b entry. Let, also, $y \in \Re$ be the displacement of the spring relative to the i_d floor and define the *connectivity* vector by $\mathbf{R}_c$=$\mathbf{R}_d$-$\mathbf{R}_b$. With this notation the force of the spring k_d and dashpot c_d are $k_d y(t)$ and $c_d \dot{y}(t)$, respectively, the inerter force is

$b\left[\ddot{y}(t)+\mathbf{R}_c\ddot{\mathbf{x}}_s(t)\right]$ and the force of the dashpot c_b is $c_b\left[\dot{y}(t)+\mathbf{R}_c\dot{\mathbf{x}}_s(t)\right]$. The total forces transferred to the host structure by the spring/dashpot and inerter/dashpot parallel combinations are, respectively,

$$f_d(t)=c_d\dot{y}(t)+k_d y(t) \tag{1}$$

$$f_b(t)=b\left[\ddot{y}(t)+\mathbf{R}_c\ddot{\mathbf{x}}_s(t)\right]+c_b\left[\dot{y}(t)+\mathbf{R}_c\dot{\mathbf{x}}_s(t)\right]. \tag{2}$$

Note that for m_d=0 these forces end up being equal and opposite (equilibrium of the connection of the two parallel combinations).

The coupled equations of motion of the structure with the inerter-based protective device are finally

$$\begin{aligned}\left(\mathbf{M}_s+\mathbf{R}_d m_d\mathbf{R}_d^T+\mathbf{R}_c b\mathbf{R}_c^T\right)\ddot{\mathbf{x}}_s(t)+\left(\mathbf{R}_d m_d+\mathbf{R}_c b\right)\ddot{y}(t)+(\mathbf{C}_s+\mathbf{R}_c c_b\mathbf{R}_c^T)\dot{\mathbf{x}}_s(t)\\ +\mathbf{R}_c c_b\dot{y}(t)+\mathbf{K}_s\mathbf{x}_s(t)=-\left(\mathbf{M}_s+\mathbf{R}_d m_d\mathbf{R}_d^T\right)\mathbf{R}_s\ddot{x}_g(t)\end{aligned} \tag{3}$$

$$(m_d+b)\ddot{y}(t)+\left(m_d\mathbf{R}_d^T+b\mathbf{R}_c^T\right)\ddot{\mathbf{x}}_s(t)+(c_d+c_b)\dot{y}(t)+c_b\mathbf{R}_c^T\dot{\mathbf{x}}_s(t)+k_d y(t)=-m_d\mathbf{R}_d^T\mathbf{R}_s\ddot{x}_g(t)\ , \tag{4}$$

where $\mathbf{M}_s\in\Re^{nxn}$, $\mathbf{C}_s\in\Re^{nxn}$, and $\mathbf{K}_s\in\Re^{nxn}$ are the mass, damping, and stiffness matrices of the host building structure, respectively, $\mathbf{R}_s\in\Re^n$ is the earthquake influence coefficient vector (vector of ones), and a dot over a symbol denotes differentiation with respect to time *t*. Furthermore, the dimensionless frequency ratio r_d, damping ratios ζ_d and ζ_b, inertance ratio β and mass ratio μ are defined as

$$r_d=\sqrt{\frac{k_d}{(m_d+b)}}/\omega_1;\quad \zeta_d=\frac{c_d}{2(m_d+b)\omega_d};\quad \zeta_b=\frac{c_b}{2(m_d+b)\omega_d};\quad \beta=\frac{b}{M};\quad \mu=\frac{m_d}{M}, \tag{5}$$

where ω_1 and M are the fundamental natural frequency and the total mass of the host structure, respectively, and $\omega_d=r_d\omega_1$ represents the IVA natural frequency based on Eq. (4). These dimensionless ratios are considered, ultimately, as the design variables in the optimization problem leading to design vector, representing the controllable parameters of the IVA, defined as

$$\boldsymbol{\varphi}=\begin{bmatrix} r_d\\ \zeta_d\\ \zeta_b\\ \beta\\ \mu\end{bmatrix}. \tag{6}$$

Note that not all components of $\boldsymbol{\varphi}$ are present for the different devices examined here (some are by default zero). This definition of design variables is consistent with what has been adopted so far in the literature for the examined here devices [6, 7, 9].

3. Modeling assumptions and response statistics calculation

3.1 Modeling assumptions and state space description

The design of building structures against earthquakes requires appropriate description of the stochastic characteristics of the seismic excitation [31]. For structural control design applications this is commonly established [43-46] by modeling ground motion $\ddot{x}_g$ as stationary Gaussian processes with spectral density $S_g(\omega)$, where ω denotes frequency. This modelling approach is equivalent to describing $\ddot{x}_g$ as a stationary filtered Gaussian white noise stochastic process and is the one adopted here. The implications of this assumption to the performance of the controlled building structures are further examined in Section 6 within the context of the illustrative example. To solve the associated random vibration problem (since excitation is stochastic process) and estimate ultimately the stationary response statistics of the structure, required in the solution of the optimum design problem outlined in the next section, a state-space formulation is adopted here. Note that such a state-space approach is the preferred one from computational perspective for linear random vibration problems [46, 47].

In this setting (i.e., using a state-space formulation for solving the random vibration problem), the excitation model is described by

$$\begin{aligned}\dot{\mathbf{x}}_q(t) &= \mathbf{A}_q\mathbf{x}_q(t) + \mathbf{E}_q w(\mathrm{t})\\ \ddot{x}_g(t) &= \mathbf{C}_q\mathbf{x}_q(t),\end{aligned} \tag{7}$$

where $w(t)\in\Re$ is a zero-mean Gaussian white-noise process with spectral intensity equal to $S_w=1/(2\pi)$, $\mathbf{x}_q(t)\in\Re^{n_q}$ is the state vector for the excitation, $\mathbf{A}_q\in\Re^{n_q x n_q}$, $\mathbf{E}_q\in\Re^{n_q x 1}$ and $\mathbf{C}_q\in\Re^{1 x n_q}$ are the state-space excitation matrices, chosen so that state-space model of Eq. (7) leads to output $\ddot{x}_g$ having desired spectral description $S_g(\omega)$. Combining excitation model of Eq. (7) with the equations of motion of the structural system in Eqs. (3) and (4) provides the augmented state-space system

$$\begin{aligned}\dot{\mathbf{x}}(t) &= \mathbf{A}(\boldsymbol{\varphi})\mathbf{x}(t) + \mathbf{E}(\boldsymbol{\varphi})w(\mathrm{t})\\ \mathbf{z}(t) &= \mathbf{C}(\boldsymbol{\varphi})\mathbf{x}(t),\end{aligned} \tag{8}$$

where $\mathbf{x}(t)\in\Re^{n_x}$ is the state vector with $n_x=2n+2+n_q$; $\mathbf{z}(t)\in\Re^{n_z}$ is the response output of the system with z_i denoting the i^{th} output; and $\mathbf{A}(\boldsymbol{\varphi})$, $\mathbf{E}(\boldsymbol{\varphi})$, $\mathbf{C}(\boldsymbol{\varphi})$ are the state-space matrices that are a function of vector $\boldsymbol{\varphi}$. Vector $\mathbf{z}(t)$ includes all variables used in formulating the IVA design problem; in this study it consists of storey drifts and floor accelerations used to describe seismic building performance [48], as well as the forces transferred by the IVA to the host structure $f_d(t)$ and $f_b(t)$ in Eqs. (1) and (2). Note that the proposed formulation takes into account the spectral characteristics of the stochastic excitation, by appropriate

augmentation of the state equation [46]. This allows for an efficient calculation of the response statistics for the augmented system. The derivation of the state-space matrices is outlined in Appendix A.

3.2 Response statistics determination

Under the modelling assumptions discussed above, the output of the system $\mathbf{z}(t)$ is a Gaussian vector process with zero-mean and covariance matrix given by

$$\mathbf{K_{zz}}(\boldsymbol{\varphi}) = \mathbf{C}(\boldsymbol{\varphi})\mathbf{P}(\boldsymbol{\varphi})\mathbf{C}(\boldsymbol{\varphi})^T;\ \ \mathbf{A}(\boldsymbol{\varphi})\mathbf{P}(\boldsymbol{\varphi}) + \mathbf{P}(\boldsymbol{\varphi})\mathbf{A}(\boldsymbol{\varphi})^T + \mathbf{E}(\boldsymbol{\varphi})\mathbf{E}(\boldsymbol{\varphi})^{\mathrm{T}} = 0\,. \tag{9}$$

where $\mathbf{P}(\boldsymbol{\varphi})$ is the state covariance matrix, obtained, by the solution of the following algebraic Lyapunov equation [47].

$$\mathbf{A}(\boldsymbol{\varphi})\mathbf{P}(\boldsymbol{\varphi}) + \mathbf{P}(\boldsymbol{\varphi})\mathbf{A}(\boldsymbol{\varphi})^T + \mathbf{E}(\boldsymbol{\varphi})\mathbf{E}(\boldsymbol{\varphi})^{\mathrm{T}} = 0\,. \tag{10}$$

The variance of each of the n_z system output variables $z_i = \mathbf{n}_i^T\mathbf{z}$ (i=1,2,…,n_z) is given by the diagonal elements of $\mathbf{K_{zz}}$ expressed as

$$\sigma_{z_i}^2(\boldsymbol{\varphi}) = \mathbf{n}_i^T\mathbf{C}(\boldsymbol{\varphi})\mathbf{P}(\boldsymbol{\varphi})\mathbf{C}(\boldsymbol{\varphi})^T\mathbf{n}_i \tag{11}$$

where $\mathbf{n}_i$ is a n_z dimensional vector of zeros with the i_{th} component being one.

In earthquake engineering applications, performance is typically quantified through the probability that EDPs (i.e., the peak of structural response quantities indicative of seismic damage such as storey drifts and floor accelerations) exceed acceptable thresholds specified by relevant seismic design codes [5, 48]. This probability can be used to evaluate the fragility of different damageable components of the structure, and for stationary excitation conditions is expressed through the out-crossing statistics rather than second-order (variance) response statistics. The probability that some output z_i exceeds threshold β_i (defining acceptable performance) within some time-window T representing the duration of the strong part of a typical seismic ground motion, is defined as

$$P_i(\boldsymbol{\varphi}\,|\,\beta_i, T) = P\Big[\big|z_i(\tau)\big| > \beta_i \text{ for some } \tau \in [0,T]\Big]. \tag{12}$$

It can be calculated as the first-passage probability for output z_i out-crossing threshold β_i. Under the stationarity assumption, the considered probability is approximated by [49]

$$P_i(\boldsymbol{\varphi}\,|\,\beta_i, T) = \ 1 - \mathrm{e}^{-\nu_i^+(\boldsymbol{\varphi})T};\ \ \nu_i^+(\boldsymbol{\varphi}) = \lambda_i(\boldsymbol{\varphi})r_i^+(\boldsymbol{\varphi})\,, \tag{13}$$

where

$$\nu_i^+(\boldsymbol{\varphi}) = \lambda_i(\boldsymbol{\varphi})r_i^+(\boldsymbol{\varphi})\,, \tag{14}$$

is the conditional out-crossing rate for z_i given by the product of Rice's unconditional out-crossing rate, $r_i^+(\boldsymbol{\varphi})$ [50], and of the temporal-correlation correction factor $\lambda_i(\boldsymbol{\varphi})$. The latter is heuristically introduced to address correlation between out-crossing events [47]. Further details for the estimation of these two factors are included in Appendix B.

4. Multi-objective design framework

4.1 Selection of performance objectives

The proposed multi-objective design framework considers two different objectives, one associated with the level of vibration suppression for the controlled building structure and one associated with the size of the (control) forces exerted by IVA to the building.

The first objective is defined following current performance-based earthquake engineering standards [5, 51] as the consequences related to different failure modes of the structure. Each of these modes corresponds to a particular response output z_i related to the building response exceeding acceptable threshold β_i and is quantified through probability $P_i(\boldsymbol{\varphi}\,|\,\beta_i,T)$, whose estimation was discussed in Section 3.2. To formalize this concept, let $\mathbf{i}_f$ represent the index set associated with the failure modes under consideration and n_f the total number of failure modes examined. Note that response vector $\mathbf{z}$ may contain additional response outputs, beyond the ones required for estimation of the occurrence probabilities of the different failure modes. In other words, n_f is not necessarily equal to n_z. The design objective, J_P, is given by the combination of probabilities $P_i(\boldsymbol{\varphi}\,|\,\beta_i,T)$ over set $\mathbf{i}_f$

$$J_P(\boldsymbol{\varphi}) = \sum_{i\in\mathbf{i}_f} w_i P_i(\boldsymbol{\varphi}\,|\,\beta_i,T)\,, \tag{15}$$

where w_i are weights representing the relative consequences for each failure mode. Estimation of objective J_P requires calculation of the out-crossing rates $\nu_i(\boldsymbol{\varphi})$ which entails a component, the temporal correction factor, $\lambda_i(\boldsymbol{\varphi})$, numerically estimated as detailed in Appendix B. Even if this correction factor is ignored, obtaining derivative information for $\nu_i(\boldsymbol{\varphi})$ can be only numerically performed [46]. This greatly increases complexity of the associated design optimization, which is one reason that such reliability-based criteria, though evidently more closely related to objectives set by current performance-based engineering practices, are not widely utilized in structural control applications [46].

To further examine the impact of the chosen design objective on the performance of the controlled structure, a variant problem is also examined, adopting the second-order statistics to characterize the level of vibration suppression. This corresponds to an analytically tractable measure given by the weighted sum of variances of output $\mathbf{z}$. As discussed in the introduction such quantification of stochastic performance

directly though variance statistics is the common approach adopted for design of IVAs. To facilitate here a consistent comparison to J_P only components of $\mathbf{z}$ belonging in set $\mathbf{i}_f$ are examined, whereas each performance variable is normalized by corresponding threshold β_i, and is given priority based on consequence weight w_i. This leads to design objective

$$J_{\mathcal{H}_2}(\boldsymbol{\varphi}) = \sum_{i\in\mathbf{i}_f} w_i^2 \frac{\sigma_{z_i}^2(\boldsymbol{\varphi})}{\beta_i^2} = \sum_{i\in\mathbf{i}_f} \frac{w_i^2}{\beta_i^2}\sigma_{z_i}^2(\boldsymbol{\varphi}), \tag{16}$$

where $\sigma_{z_i}^2(\boldsymbol{\varphi})$ is the response variance of output z_i given by Eq. (11).

In the linear control theory literature, this measure is associated with $\mathcal{H}_2$ optimal control (when the problem is posed deterministically, in the frequency domain), or as Linear Quadratic Gaussian (LQG) control (when it is posed stochastically). In the interest of brevity, we will refer to $J_{\mathcal{H}_2}(\boldsymbol{\varphi})$ as the $\mathcal{H}_2$ measure. This measure is analytically tractable with computation of derivative information also being straight-forward [52]. Thus, its adoption greatly simplifies the associated design optimization compared to the reliability-based objective function in Eq.(15).

The second objective herein adopted relates to the control forces exerted by the IVA to the building structure to account for potential local strengthening of the structure required for the safe transmission of these forces. For the TID and the TMVD either f_b or f_d can be used for this purpose, since they are equal in magnitude. For the TMDI, though, differences may exist between these two forces since equilibrium between them is established based on Eq. (4) by also considering the inertia forces associated with the absolute acceleration of mass m_d. To establish a common secondary objective for all devices, the maximum between forces f_b and f_d is adopted, that is the maximum force transferred to at any of the two ends of the device to the building. Since under the stated stationary assumptions the peak response for z_i can be approximated by the product of stationary variance $\sigma_{z_i}^2$ times a constant, the peak factor [53], the maximum of the standard deviation of forces f_b and f_d is taken as the second design objective. That is,

$$J_2(\boldsymbol{\varphi}) = \max\left\{\sigma_{f_b}, \sigma_{f_d}\right\}, \tag{17}$$

in which the standard deviations σ_{f_b} and σ_{f_d} are readily obtained through Eq. (11). Note that consideration of the device forces as design objective may be also interpreted as an approach to incorporate in the design cost-characteristics of the IVA [36], since cost of many type of passive vibration control devices relates well to their peak force demand/capacity [54]. The devices considered here, though, consist of several devices/components, such as connectors (springs), viscous dampers (dashpots), and inerters, with fundamentally different relationships between force demand and cost. More importantly, contrary to linear dampers, inerter devices are not currently commercially available for large-scale civil engineering

applications. In this regard, no dependable force-cost relationship for the case of the inerter element/device yet exists and, consequently, no such relationship may be dependably established for the considered IVAs. Therefore, the adoption of IVA forces as design objective is primarily addressing the strengthening required to accommodate the transfer of these forces and may not necessarily scale-up with the overall IVA cost.

4.2 Multi-objective design problem formulation

The multi-objective design problem is finally formulated by considering concurrently the design objectives in the previous section as

$$\boldsymbol{\varphi}^* = \arg\min_{\boldsymbol{\varphi}\in\Phi} \left\{ J_1(\boldsymbol{\varphi}), J_2(\boldsymbol{\varphi}) \right\}^T, \tag{18}$$

where first objective $J_1(\boldsymbol{\varphi})$ corresponds to either J_P given by Eq. (15) or $J_{\mathcal{H}_2}$ given by Eq. (16), and Φ represents the admissible design space, defined by considering appropriate box-bounded constraints for each of the design variables in vector $\boldsymbol{\varphi}$. Since the two design objectives are competing there is no design configuration that simultaneously minimizes them both. The design optimization problem is transformed to identification of the *Pareto optimal* solutions, also known as dominant designs. A design configuration is Pareto optimal, denoted $\boldsymbol{\varphi}_p$, if there is no other configuration that improves one objective without detriment to the other. The set of all such configurations is denoted as the *Pareto set* $\boldsymbol{\Phi}_p$. *The Pareto front* is the representation of the Pareto set in the objective function space $\mathbf{J}_p = \{[J_1(\boldsymbol{\varphi})\ J_2(\boldsymbol{\varphi})] \,|\, \boldsymbol{\varphi} \in \boldsymbol{\Phi}_p\}$. Examples of such Pareto fronts will be provided in the illustrative example considered later. It is generally impractical to find all Pareto optimums so the optimization strategies usually aim at finding a subset of them that represents $\mathbf{J}_p$ well and can provide the decision maker with a comprehensive picture of trade-offs [55]. To this end, the multi-objective design problem aims to identify a range of design configurations (Pareto optimal solutions) striking a trade-off among (i) vibration suppression efficiency and (ii) strengthening required for accommodating the force transferred by IVA to the controlled building structure. The designer or decision maker (e.g. building owner) can ultimately make the final decision among the Pareto optimal solutions, incorporating any additional considerations including architectural constraints in implementing different IVA configurations.

4.3 Solution to multi-objective problem

The multi-objective optimization problem of Eq. (18) is solved by the epsilon-constraint method [56]. This numerical optimization approach is preferred here due to its ability to discover nonconvex regions of the Pareto front (compared to, for example, the weighted sum approach) and the fact that it can provide a front with a pre-determined resolution (compared to, for example, evolutionary approaches). Without loss of generality, objective $J_1(\boldsymbol{\varphi})$ is used as *optimization function* and objective $J_2(\boldsymbol{\varphi})$ as *constraint function*. The epsilon-constraint method converts the multi-objective optimization problem to a set of single-objective constraint optimization problems with different constraints ε^r

$$\boldsymbol{\varphi}_p^r = \arg\min_{\boldsymbol{\varphi}\in\Phi} J_1(\boldsymbol{\varphi}) \quad \text{such that} \quad J_2(\boldsymbol{\varphi}) \le \varepsilon^k, \tag{19}$$

where the superscript k is utilized to describe the k-th such constraint. Systematic variation of ε^r facilitates identification of the Pareto front. The formulation of Eq. (19) allows ultimately the identification of design configurations for optimal seismic protection of building structure while maintaining the device forces below the target threshold of ε^k. Optimization problem of Eq. (19) corresponds to a nonlinear, constrained optimization problem and can be solved through any appropriate numerical technique. In this study it is solved using the powerful optimization environment TOMLAB [57].

For deciding the range for ε^r the anchor point of the Pareto front corresponding to the maximum of $J_2(\boldsymbol{\varphi})$ is first obtained by solving of the unconstrained single objective-optimization

$$\boldsymbol{\varphi}_1^{an} = \arg\min_{\boldsymbol{\varphi}\in\Phi} J_1(\boldsymbol{\varphi}). \tag{20}$$

The maximum value for $J_2(\boldsymbol{\varphi})$ across the front is $J_2(\boldsymbol{\varphi}_1^{an})$. The minimum is equal to zero (uncontrolled structure, corresponding to the other anchor point of the Pareto front). The range for feasible epsilon constraints ε is therefore $[0\ J_2(\boldsymbol{\varphi}_1^{an})]$. If n_p equally spaced solutions are desired, then each ε^r is chosen as

$$\varepsilon^k = \frac{k}{n_p} J(\boldsymbol{\varphi}_1^{an});\ k = 1,...,n_p. \tag{21}$$

Evidently, for $k=n_p$ the optimal configuration is $\boldsymbol{\varphi}_1^{an}$ whereas for $k=0$ (i.e. corresponding to the other anchor point of the front) the solution corresponds to the uncontrolled structure (zero forces).

5. Illustrative case-study

The proposed design approach is illustrated in this section by considering a 9-storey steel moment resisting frame (MRF) building as the structure to be controlled. The structure is one of those considered in the third generation of structural control benchmark problems [41], and has been adopted as illustrative application in a number of studies examining the efficiency of different seismic protective devices (see for example, [58, 59]).

5.1 Structural and excitation models

The stationary seismic excitation $\ddot{x}_g$ is described by a high-pass filtered Kanai-Tajimi power spectrum [31]:

$$S_g(\omega) = s_o \frac{\omega_g^4 + 4\zeta_g^2\omega^2\omega_g^2}{\left(\omega_g^2-\omega^2\right)^2 + 4\zeta_g^2\omega_g^2\omega^2} \frac{\omega^4}{\left(\omega_f^2-\omega^2\right)^2 + 4\zeta_f^2\omega_f^2\omega^2}\ . \tag{22}$$

In the above equation the Kanai-Tajimi parameters ω_g and ζ_g represent the stiffness/frequency and damping properties, respectively, of the supporting ground modeled by a linear damped SDOF oscillator excited (at the bedrock) by white noise. Further, the parameters ω_f and ζ_f control the cut-off frequency and the "steepness" of a high-pass filter used to suppress the low frequency content allowed by the Kanai-Tajimi filter. Lastly, s_o is chosen to achieve a desired pre-specified value for the root mean square ground acceleration a_{RMS} of the considered seismic input. The state-space representation of this excitation model is given in Appendix A. For the purposes of this study parameters ω_g, ω_f , ζ_g and ζ_f of the filtered Kanai-Tajimi seismic input spectrum in Eq. (22) are taken to have values $\omega_g=3\pi$, $\omega_f=\pi/2$, $\zeta_g=0.4$ and $\zeta_f=0.8$, representing soft soil conditions [31] whereas the intensity of the excitation is taken as $a_{RMS}=0.06g$, where $g=9.81$ m/s^2 is the gravitational acceleration, representing moderate intensity. This selection leads to value of s_o equal to 0.0063 m^2/s^3. The strong ground motion duration T is taken as 15 s.

The 9-storey structure has a rectangular plan with dimension 45.73 m with lateral load resisting system comprised of two (perimeter), five-bay steel moment-resisting frames (MRFs). First floor height is 5.49 m while height of all other floors is 3.96 m. The seismic mass of the structure (defining mass matrix $\mathbf{M}_s$) is 1.01×10^6 kg for the first storey, 9.89×10^5 kg for the second through eighth storeys and 1.07×10^6 kg for the ninth storey. The total seismic mass of the structure is 9.00×10^6 kg. Analysis is performed along the NS direction of the structure and the corresponding stiffness matrix, $\mathbf{K}_s$, is obtained through static condensation of the structural model detailed in [41]. Natural periods (and participating modal mass ratios in parenthesis) for the first three modes are 2.27s (82.8%), 0.85s (10.9%) and 0.49s (3.4%) respectively. For defining the damping matrix $\mathbf{C}_s$ modal damping equal to 2% is assumed for all modes of vibration [31]. Further details for the benchmark structure, including plan and elevation views may be found in [41].

5.2 Performance quantification and details for implementations examined

A total of 18 building performance variables are used in the IVA optimal design problem which include all 9 above-ground storey drifts and absolute floor accelerations with thresholds taken as 1.5% of story height, for the drifts, and 0.45g for the accelerations. These thresholds are selected to represent moderate failure modes for steel MRFs and structural contents, respectively [6]. Without loss of generality, equal weights $w_i=1/n_f$ are considered for all the building performance variables. This assumes equal consequences for all failure modes and was chosen to provide a comparable contribution to J_P by the drift and acceleration related failure modes. The value of J_P for the uncontrolled structure is 20.1%. When considering only drift or acceleration responses this value becomes 20% and 20.2%, respectively.

Placement of a single IVA (i.e., either TVMD, TMDI, or TID in Figure 1) is considered either at the ground (1st) storey or at higher stories: top (9th) story and penultimate (8th) story. The former IVA location choice is justified by the fact that TID was found to perform better when placed at the ground storey of buildings in previous studies [6, 32]. The latter IVA location is motivated by the fact that conventional

TMDs tuned to suppress the first (dominant) mode of building structures are commonly attached to the top floors [4, 33]. Furthermore, an additional placement in which IVAs span the two highest floors is also examined inspired, as discussed in Section 2, by pendulum type of TMD implementations in buildings with large slab opening allowing suspension of secondary mass using cables longer than a single storey height (see e.g., Taipei 101). In summary, the following 4 IVA placements are examined, codified in terms of i_d and i_b values shown in Figure 1 as (a) i_d=9 and i_b=8, (b) i_d=8 and i_b=7, (c) i_d=9 and i_b=7 and (d) i_d=1– i_b=0. Hereafter, these placements will be referenced as "top-storey", "8th-storey", "9/7-storeys", and "1st-storey", respectively.

5.3 Details for design optimization and applications examined

The admissible design space is taken to be [0.005 10] for ζ_d and ζ_b, [0.1 3] for r_d, [0 5] for β and [0.001 0.05] for μ. Optimal TMDI design is undertaken by treating the mass ratio μ as a design variable as well as by taking it fixed to μ=0.01 (case denoted as TMDI$_m$). The latter case is intended to investigate applications for which the TMDI is used as a retrofit measure to an existing TMD installation, for which explicit optimization of μ is not possible. Note that for the case of the TVMD larger values have been proposed in the literature for optimal tuning ratio than the upper bound r_d=3 utilized here [35]. For such values, though, the TVMD gradually starts behaving more like a diagonal bracing (stiff element) rather than as an energy dissipation mechanism as intended [7]. The range for r_d was chosen so that optimal implementation maintains the tuning as viscous mass damper [7], though in all instances the optimization converged to the boundary of the considered range leading to r_d=3. The range of the mass ratio was chosen based on practical considerations about the feasible mass to facilitate a mass damper implementation (choice of lower bound) without excessively increasing gravity loads of the structure (choice of upper bound). For the remaining design variables, the admissible bounds were chosen to avoid convergence to their respective boundaries.

Two different *formulations* of the multi-objective design problem are considered. The main one adopts J_1=J_P as objective for quantifying vibration suppression efficiency and is referenced herein as D_p design. The variant adopts J_2= $J_{\mathcal{H}_2}$ and is referenced herein as D_v design. Moreover, three different optimal IVA *design applications* are investigated with respect to the performance variables of the benchmark building. One application includes only the 9 storey drifts in the $\mathbf{i}_f$ set in Eqs. (15) and (16) as performance variables referenced hereafter as *drift-sensitive* design, while a second application, referenced as *acceleration-sensitive* design, takes only the 9 floor accelerations as performance variables in the $\mathbf{i}_f$ set. The drift-sensitive and the acceleration-sensitive designs are readily implemented by setting weights w_i=0 to all floor accelerations and to all storey-drifts, respectively, in defining the objective functions in Eqs.(15) and (16), while the remainder of the weights are set equal to w_i=1/n_f =1/9. The third design application utilizes all storey drifts *and* floor accelerations as performance variables in the $\mathbf{i}_f$ set in Eqs. (15) and (16) equally weighted by w_i=1/n_f=1/18 and is referenced as *balanced* design in what follows.

5.4 Results and discussion

The presentation and discussion starts from the computationally more involved D_p problem formulation and balanced design. Figures 2 and 3 show, respectively, the Pareto front and Pareto optimal solutions for top-storey placement for all different IVAs considered. The Pareto optimal solutions are plotted in Figure 3 as a function of objective J_2, whereas for objective J_1 (corresponding to J_P in this case) both linear and logarithmic scales are used in Figure 2. The logarithmic scale is chosen to depict better differences across the entire front, since the variation of J_P is significant (order of magnitude difference between maximum and minimum values of J_P).

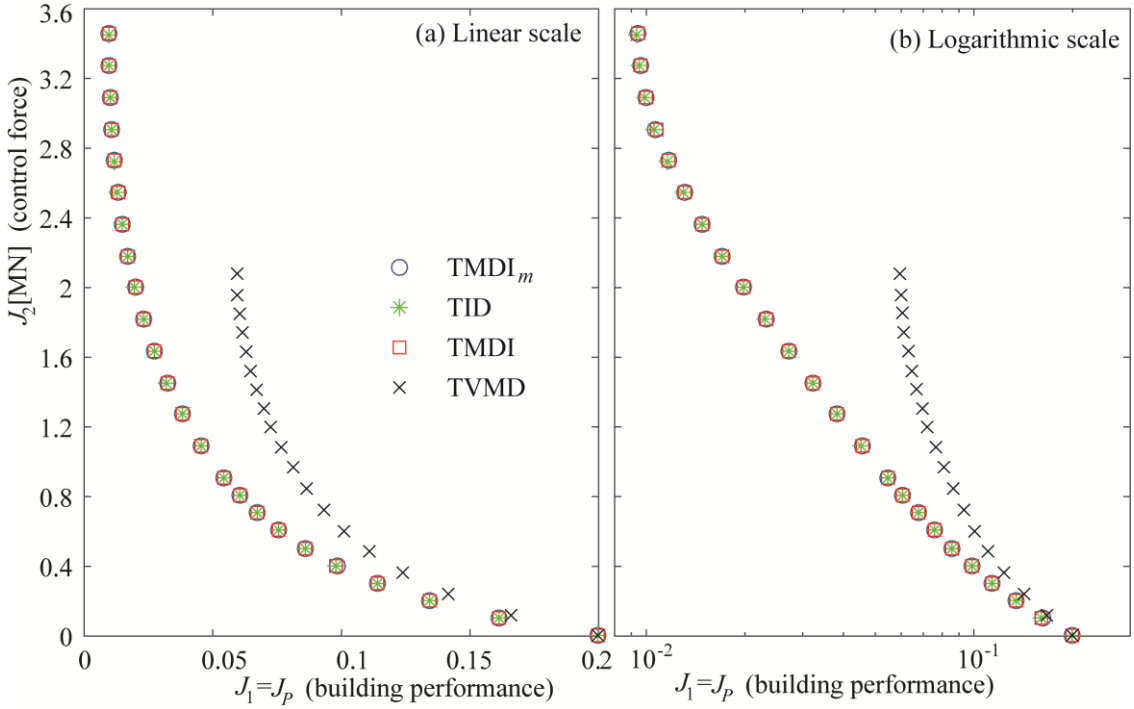

Figure 2: Pareto front for D_p problem formulation, balanced design application and top-storey IVA placement plotted against objective J_1 (building performance measure) in (a) linear scale; and (b) logarithmic scale.

Commenting first on the Pareto front data in Figure 2, significant variation is seen for both objectives across the front. This demonstrates the usefulness of the proposed multi-objective design approach which pinpoints the compromise between the two competing objectives. The structural design engineer can ultimately choose a design configuration from those identified using any desired criteria. Practically meaningful design choice may be the one that requires strengthening below a desired level (constraint on J_2), or the one yielding smallest force transfer that accomplishes a specific level of performance improvement (constraint on J_1), or, perhaps more appropriately, the one that strikes a good balance between both objectives. In multi-criteria optimization, a common choice for the latter [60] is the design that in the

Pareto front has the minimum distance from the Utopia point, corresponding to the unachievable mimimum of both objectives [$J_1 = J_1(\boldsymbol{\varphi}_1^{an})$, $J_2=0$]. This distance can be estimated considering any appropriate normalization/transformation for the objectives, using, for example, either linear or logarithmic scale for J_P. Commonly, the minimum distance from the Utopia point lies close to the middle of the front which is a desired location. This is because close to the two anchor points (i.e., boundaries) of the Pareto front, small improvements in one objective are achieved with big sacrifices of the other one and, therefore, it is reasonable to argue that solutions towards the two ends (anchor points) of the Pareto front should be avoided in search for a well-balanced solution between the competing objectives.

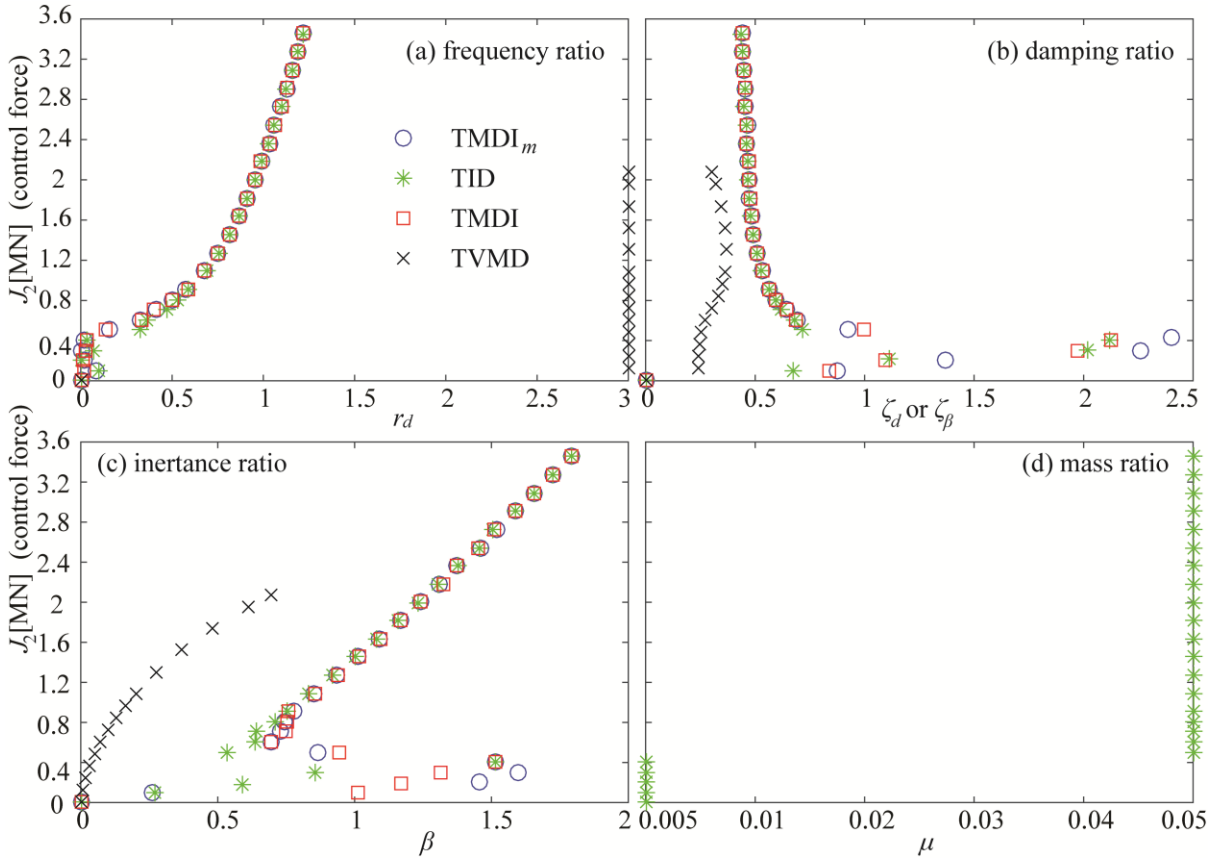

Figure 3: Design variable values of Pareto optimal solutions plotted against objective J_2 (IVA control force measure) for D_p problem formulation, balanced design application, and top-storey IVA placement

Regardless of the approach adopted to choose the final design, the Pareto fronts provide invaluable information for the compromise of the considered objectives and for shedding light on the vibration control effects provided by different optimal IVA designs. For the examined IVAs, it is evident that the vibration suppression level can be maintained close to optimal performance with an important reduction of the force transferred to the host building structure which is a critical practical design consideration. Comparison

between different types of IVAs (Figures 2 and 3) shows that TID, TMDI and TMDI$_m$ achieve practically identical performance across the entire front. This is not surprising: it has been shown that independent of the mass ratio μ a similar vibration suppression level may be established through proper tuning of the TMDI [9, 32], and that this level is close to the one achieved by the TID [32] interpreted as a special TMDI with μ=0. Only for very large mass ratios may there be a deviation from this trend [32]. This is validated here, and, more importantly, it is shown that it applies across the entire Pareto front within a multi-objective setting. The Pareto optimal design configurations are also very similar for all IVAs (Figure 3) except for relatively low control force range J_2<1MN. This can be attributed to the numerical optimization; in low control force regimes small sensitivity exists for the performance close to the Pareto optimal solution since performance improvement compared to the uncontrolled structure is small and, thus, significantly different design parameter values yield similar performance leading to convergence to different optimal designs of similar performance.

Notably, the above noted similarities in both performance and optimal design variables between TMDI and (massless) TID are also convenient from a practical design viewpoint since they show that the mass of the physical devices, which might be ignored in design (i.e., by setting m_d=0 for TID), will not alter either the performance or the design itself, even if this mass ends up being non-negligible in practice. The level of similarity of performance among TMDI, TID and TMDI$_m$ shown in Figure 2 holds for problem formulation D_y as well as for all IVA placements and design applications examined. For this reason, results for TMDI, TID and TMDI$_m$ are mostly grouped together for the rest of this paper, and referenced as TMDI/TID.

Nevertheless, the performance of TVMD is significantly different from, and lower than, the TMDI/TID (Figure 2), with lower optimal inertance values and stiffness that converges to the boundary of the feasible design region (Figure 3). As discussed in Section 5.3 the latter might be contributing to the lower performance of this particular IVA, but is essential to ensure that TVMD does not act as a mere stiffener but rather as an energy dissipator endowing supplemental damping to the building. From the perspective of the dashpot placement, the essential difference between TVMD and TMD/TID, it is evident that having the spring acting in isolation in the TVMD (without a dashpot in parallel connection) increases the force demand on it, required for the TVMD to balance the combined inerter/dashpot forces, something that yields an optimal stiffness value at the upper boundary of the design region and ultimately reduces overall device effectiveness. The comparison between TVMD and TMDI/TID is further discussed after presentation of results for the remaining implementation cases.

Next, Pareto fronts for different IVA placements within the benchmark building structure are shown in Figure 4 for D_p problem formulation and balanced design plotted against J_1 objective. For all Pareto fronts presented from this point on logarithmic scale is utilized for J_1=J_P to better illustrate differences at small

values. The characteristics with respect to the Pareto front itself are similar to the general trends observed in Figure 2, so emphasis in all discussions from now on is placed on the comparison across the different implementations cases and devices. IVA placement at lower floors improves vibration control efficiency as manifested by lower J_1 values. This trend agrees with results reported in [32, 33], but herein it is further shown that placement at lower floors reduces control force J_2 exerted to the building for the same value of J_1. Even more improved vibration suppression efficiency is achieved by allowing IVA to span two storeys in which both objectives are simultaneously reduced across the entire Pareto front. Therefore, notwithstanding architectural constraints envisioned to be more relaxed for the TMDI case, IVA placement across multiple floors should be preferred.

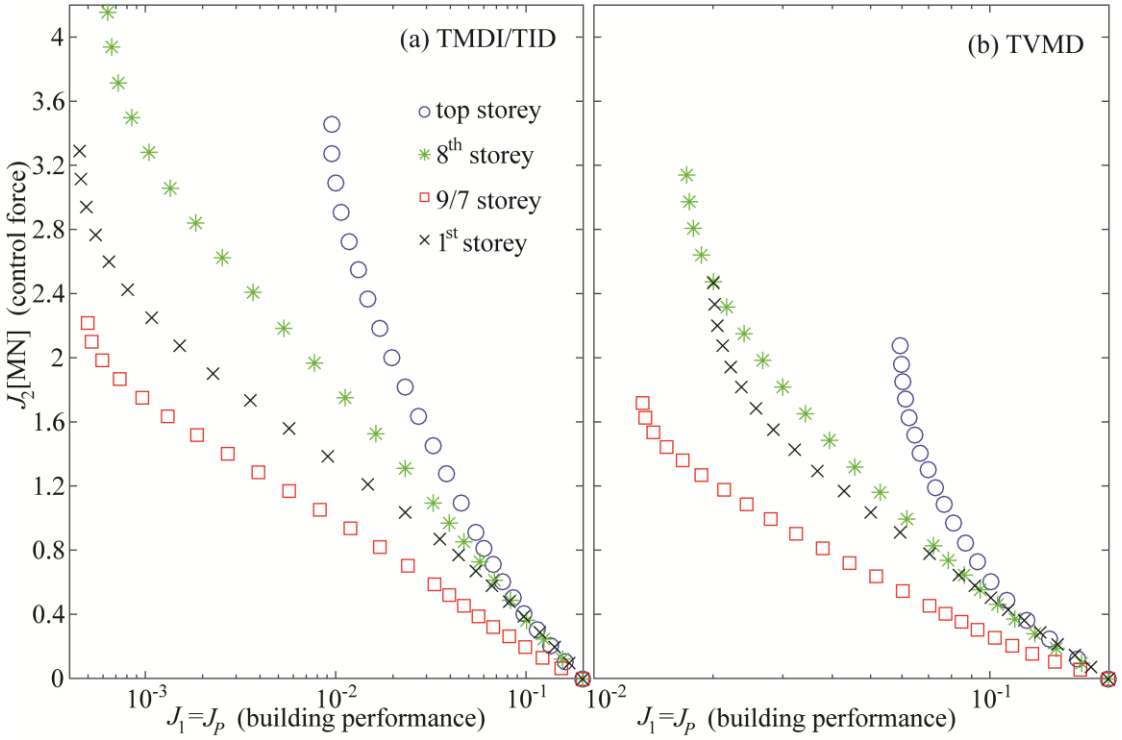

Figure 4: Pareto front for D_p problem formulation, balanced design application and different placements for (a) TMDI/TID and (b) TVMD.

Turning the attention to the ability of IVAs to suppress different building kinematics (i.e., storey drifts vis-à-vis floor accelerations), Figures 5 and 6 show Pareto fronts for acceleration-sensitive, drift-sensitive and balanced design applications for top-storey and 1st-storey IVA placement, respectively, while Figures 7 and 8 show Pareto fronts for drift-sensitive and acceleration-sensitive, respectively, designs for top-storey IVA placement (i.e., they equivalently replicate Figure 3 for the other two design applications).

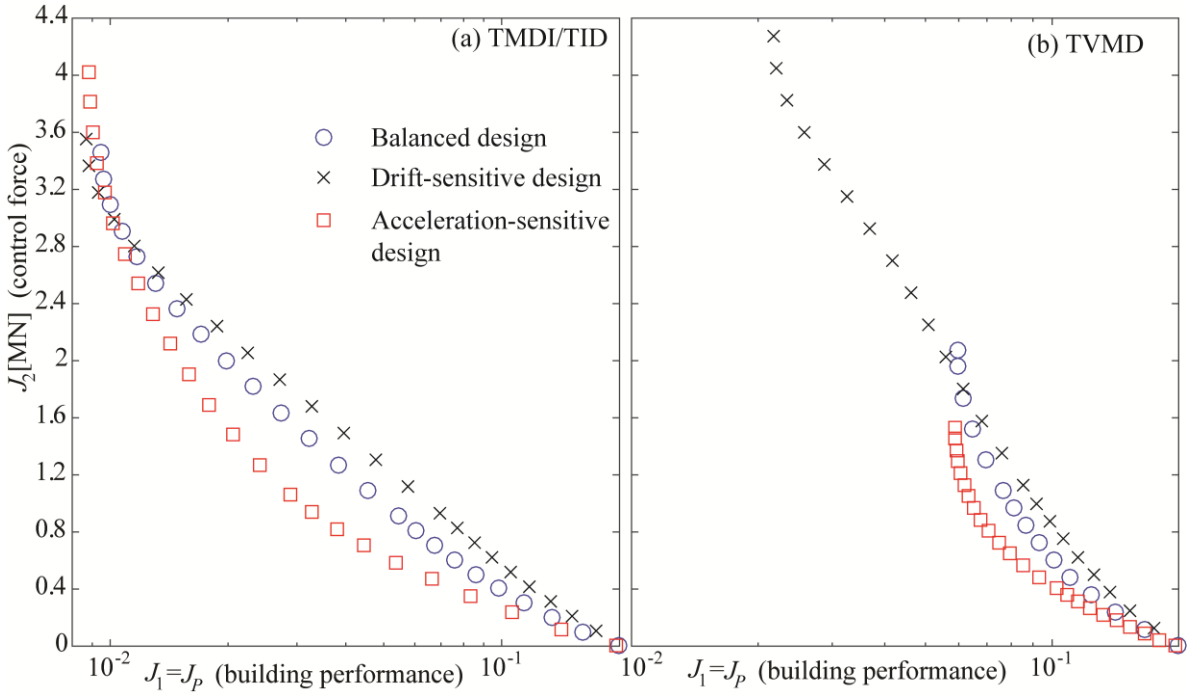

Figure 5: Pareto front for D_p problem formulation and different design applications for top-storey placement of (a) TMDI/TID and (b) TVMD.

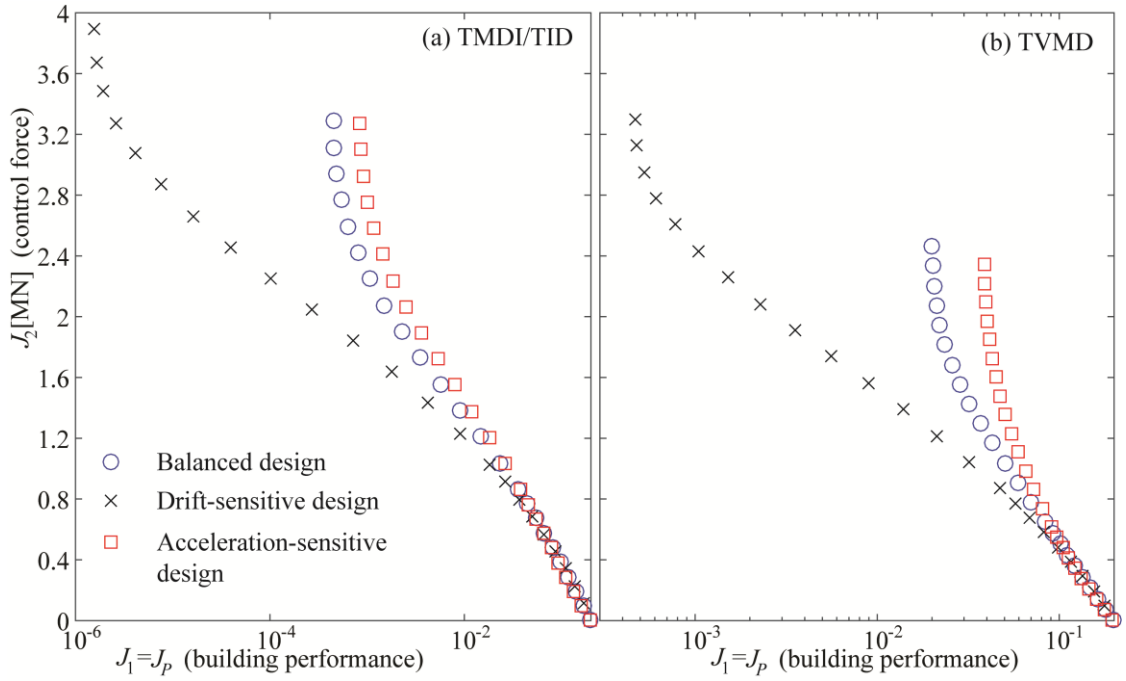

Figure 6: Pareto front for D_p problem formulation and different design applications for 1st-storey placement of (a) TMDI/TID and (b) TVMD.

It is seen that all devices exhibit superior ability to mitigate storey-drifts (drift-sensitive design application) compared to floor accelerations (acceleration-sensitive design application). This is a common limitation for most of passive control devices [2]: since accelerations are influenced by higher-order dynamics, the proper design/tuning of seismic protective devices to efficiently suppress vibration across the entire frequency range of importance for accelerations poses typically a greater challenge than deformation control dominated by a narrower (low) frequency range. The differences between acceleration and drift sensitive designs are especially evident for TVMD or for TMID/TID placed at the 1st storey. The TVMD in particular faces significant challenges in suppressing accelerations, leading to small improvement for J_1 (Figures 5, 6) and small Pareto optimal inertance values (Figure 8) for the acceleration-sensitive design application. For the drift-sensitive design application the optimal inertance values for the TVMD become even higher than the ones for the TMDI/TID, with associated higher forces (J_2 values) for some parts of the Pareto front (Figures 5, 7). The inefficiency of TVMD to suppress floor accelerations is similar to that observed for viscous dampers [2], and the fact that TVMD is a variant of viscous dampers as discussed in the introduction is no coincidence. Still, even for drift-sensitive design the performance of the TVMD is inferior to the TMDI/TID.

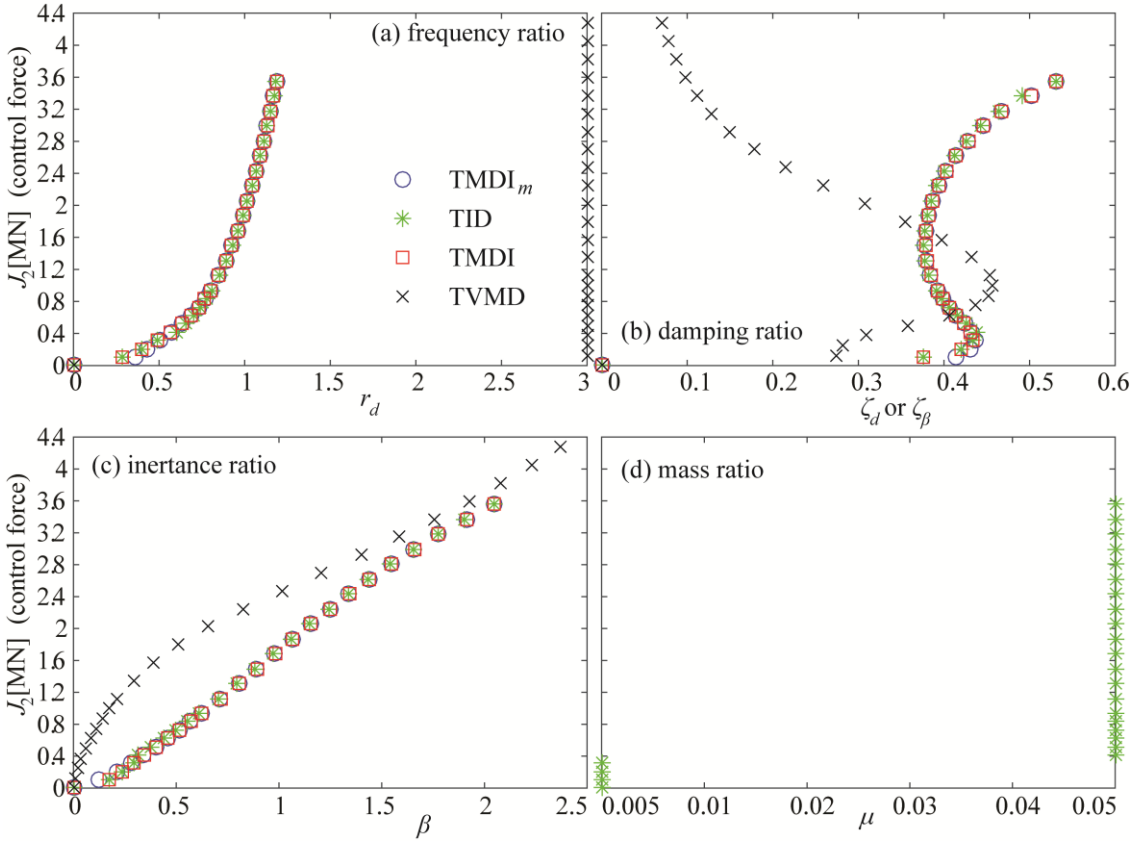

Figure 7: Design variable values of Pareto optimal solutions plotted against objective J_2 () for D_p problem formulation, drift-sensitive design application, and top-storey IVA placement.

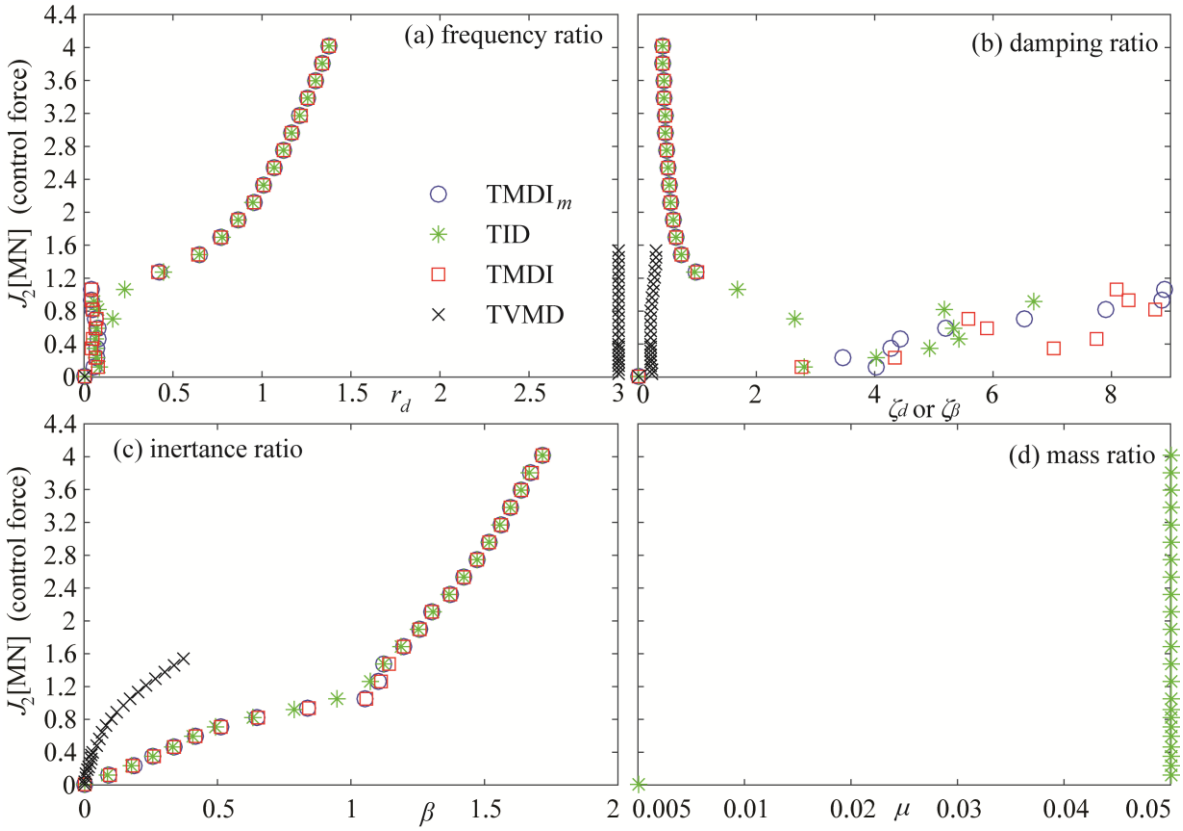

Figure 8: Design variable values of Pareto optimal solutions plotted against objective J_2 (IVA control force measure) for D_p problem formulation, acceleration-sensitive design application, and top-storey IVA placement.

Another interesting trend is that across the TMDI, TID and TMDI$_m$ implementations more significant (compared to the balanced design application in Figure 3) differences exist for Pareto optimal designs for small J_2 values for acceleration-sensitive design application while practically no difference for the drift-sensitive design application. Since such differences stem, as discussed earlier, from potential trade-offs between the different failure modes (note that performance remains the same despite these differences), this should be attributed to the sensitivity of accelerations to higher order dynamics: such a trade-off is not possible when response is dominated by the fundamental mode of the structure (since all different performance variables share same variation trends), as is the case for drifts. Overall, the herein furnished numerical data suggests a need to carefully examine the importance of the different peak response demands in seismic applications; designing for displacement/deformation quantities is not sufficient when failure modes related to accelerations may be critical. And, contrary to TMDs targeting a single (usually the first/fundamental vibration mode), TMDI/TID are very capable to mitigate concurrently storey drifts and floor accelerations achieving wideband vibration suppression (see also [32, 33]) as long as both are included in the objective function of the optimal IVA design problem.

Finally, Figure 9 examines the difference between D_p and D_v design formulations. It shows the performance achieved by both designs with respect to the J_P metric definition, which as stressed earlier is the performance metric compatible with modern performance-based earthquake engineering practices. Results for D_p correspond to the actual Pareto optimal solution while D_v case traces a sub-optimal solution that would be achieved if one adopts the simpler design approach of sum of variance minimization (but ultimately cares about performance expressed in relevant to engineering practice quantities). Results show that for domains of the Pareto front corresponding to highly efficient IVAs (i.e., small J_P values and therefore better vibration suppression) significant differences may exist. Differences are bigger for 1st-storey or TMDI/TID implementations, for which the anchor point of the front corresponding to optimal vibration suppression is associated with both higher control forces (larger J_2 value) and lower protection level (larger J_P value). This demonstrates that adoption of design objectives should be done with appropriate care; adoption of the simpler sum of variances might lead to suboptimal configurations for performance quantification that is associated with consequences of the different failure modes of the structure.

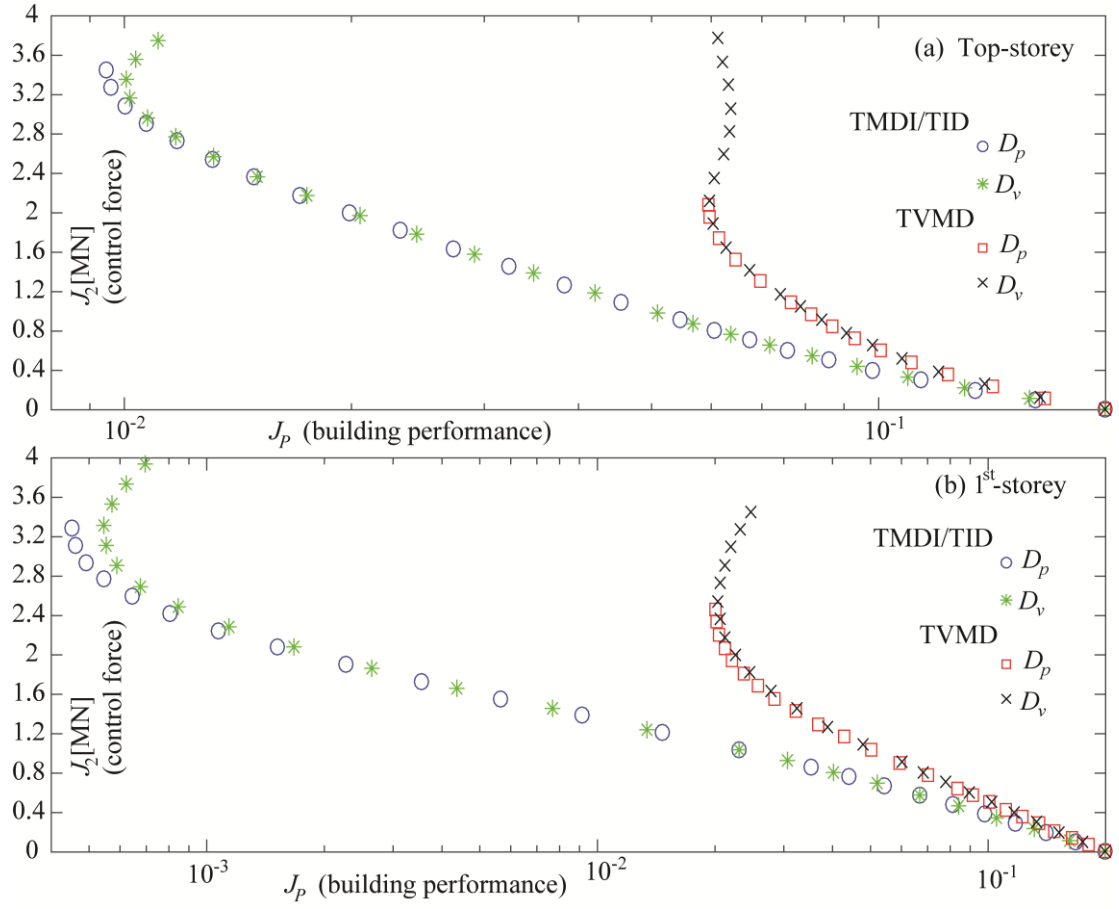

Figure 9: Comparison between D_p and D_v designs for balanced design application and IVA placement at (a) top-storey or (b) 1st-storey.

6. Optimal IVA design assessment for non-stationary seismic excitation

In the previous section, the widely-used stationary excitation model in Eq.(22) accounting for the influence of local soil conditions to the frequency content of the seismic ground motion has been employed for optimal multi-criteria IVA design. Nevertheless, typical acceleration traces of ground motions recorded during historic seismic events attain time-varying amplitude; they exhibit an initial short period of signal energy rise followed by a fully-developed in amplitude segment and a final decaying segment. Consequently, seismic structural response to actual earthquake excitations is non-stationary. In this respect, it is deemed prudent to verify whether structural response trends and optimality conditions *for IVA design purposes* previously identified under stationary excitation for the benchmark case-study building remain the same for excitation with non-stationary (evolutionary) amplitude. Rather than using recorded ground motions, which would be mostly relevant for *seismic risk assessment purposes* to an existing structure, non-stationary seismic excitation is modeled here using a stochastic ground motion modeling approach [61, 62], by modulating in time the colored stationary excitation in Eq.(22) through an analytically defined temporal envelop function. This consideration facilitates a consistent comparison between stationary excitation used in optimal IVA design and non-stationary excitation used for verification of optimal IVA design by equating the stationary excitation conditions (and duration T) with the respective characteristics of the fully-developed in amplitude segment of recorded accelerograms as detailed below.

A plethora of parametrically defined envelope functions have been proposed in the literature for capturing typical amplitude non-stationarity trends of recorded accelerograms. Herein, the commonly-used function proposed by Housner and Jennings [63] is adopted, defined by

$$e_t(t)=\begin{cases}(t/T_1)^2 & \text{for } t<T_1\\ 1 & \text{for } T_1\le t\le T_1+T_2\\ e^{-\alpha(t-T_2)} & \text{for } t>T_1+T_2.\end{cases} \tag{23}$$

The above envelope consists of a quadratic rise of duration T_1, a plateau of duration T_2 corresponding to the fully-developed in amplitude time-history segment, and an exponential decay with rate α (see also Figure 10(a)). Non-stationary time-history excitation is obtained by modifying the output equation of the state-space excitation model in Eq. (7) to be

$$\ddot{x}_g(t)=e_t(t)\mathbf{C}_q\mathbf{x}_q(t). \tag{24}$$

For numerical application, the parameters of the envelope in Eq.(23) are selected as T_1=T_2=15s and α is chosen so that the envelope value is 0.05 for t=50 s. Note that the T_2 value is equal to the stationary excitation duration T considered in the optimal IVA design for the illustrative case-study building in the previous section, so that a consistent comparison between stationary (design) and non-stationary

(verification) excitation conditions is established. The adopted envelope function and a sample synthetic ground motion acceleration time-history are plotted in Figure 10.

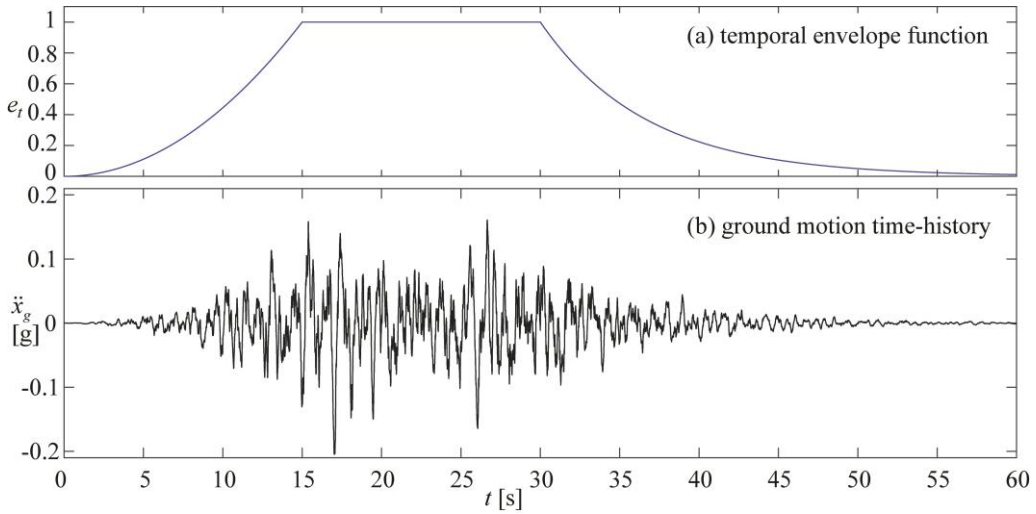

Figure 10: (a) Envelope function used for modeling non-stationary excitation and (b) sample acceleration time-history used to evaluate non-stationary response.

Figure 11 plots response time-histories of the uncontrolled benchmark building and of the same equipped with three different TMDI/TIDs Pareto optimal implementations following the D_P optimization formulation. In particular, optimal designs corresponding to the Pareto front anchor point for minimum J_1 objective (maximum vibration suppression) and top-storey or 1st-storey IVA placement are shown (second and fourth row, respectively, in Figure 11). These two cases are denoted as IVA_1 and IVA_3, respectively. For the top-storey placement, the Pareto optimal design corresponding to the minimum distance from the Utopia point is also shown (third row), denoted as IVA_2. Recall that this case represents a judicial trade-off between J_1 and J_2 objectives. The parametric configuration $\boldsymbol{\varphi}$ for the three IVA implementations is also provided in Figure 11. Outputs shown include drift for the 8th story, absolute top floor acceleration and IVA force, that is, all relevant quantities examined in the IVA optimal design. The specific stories for drifts and accelerations are selected as this is where response quantities are maximised. Note, though, that trends for all other stories are quite similar, as expected for a linear structure with a dominant fundamental mode. The trends observed in Figure 11 under the non-stationary conditions verify the trends observed for stationary excitation. The TMDI/TID provides significant response reduction compared to the uncontrolled structure: peak top-storey drift and peak top floor acceleration are reduced by at least 25% and 50%, respectively. Further, IVA placement at 1st-storey improves performance compared to top-storey placement in terms of root mean square (RMS) top-storey drift, though not in terms of peak response top-storey drift and top floor acceleration as evidenced by comparing the first two plots of 2nd and 4th rows in Figure 11. More

importantly, the Pareto optimal solution in the 3rd row of Figure 3 which strikes a good compromise between structural performance J_1 and IVA force J_2 develops three times lower peak inerter force with minor deterioration in vibration suppression as seen by comparing the plots in the 2nd vis-avis 3rd row in Figure 11.

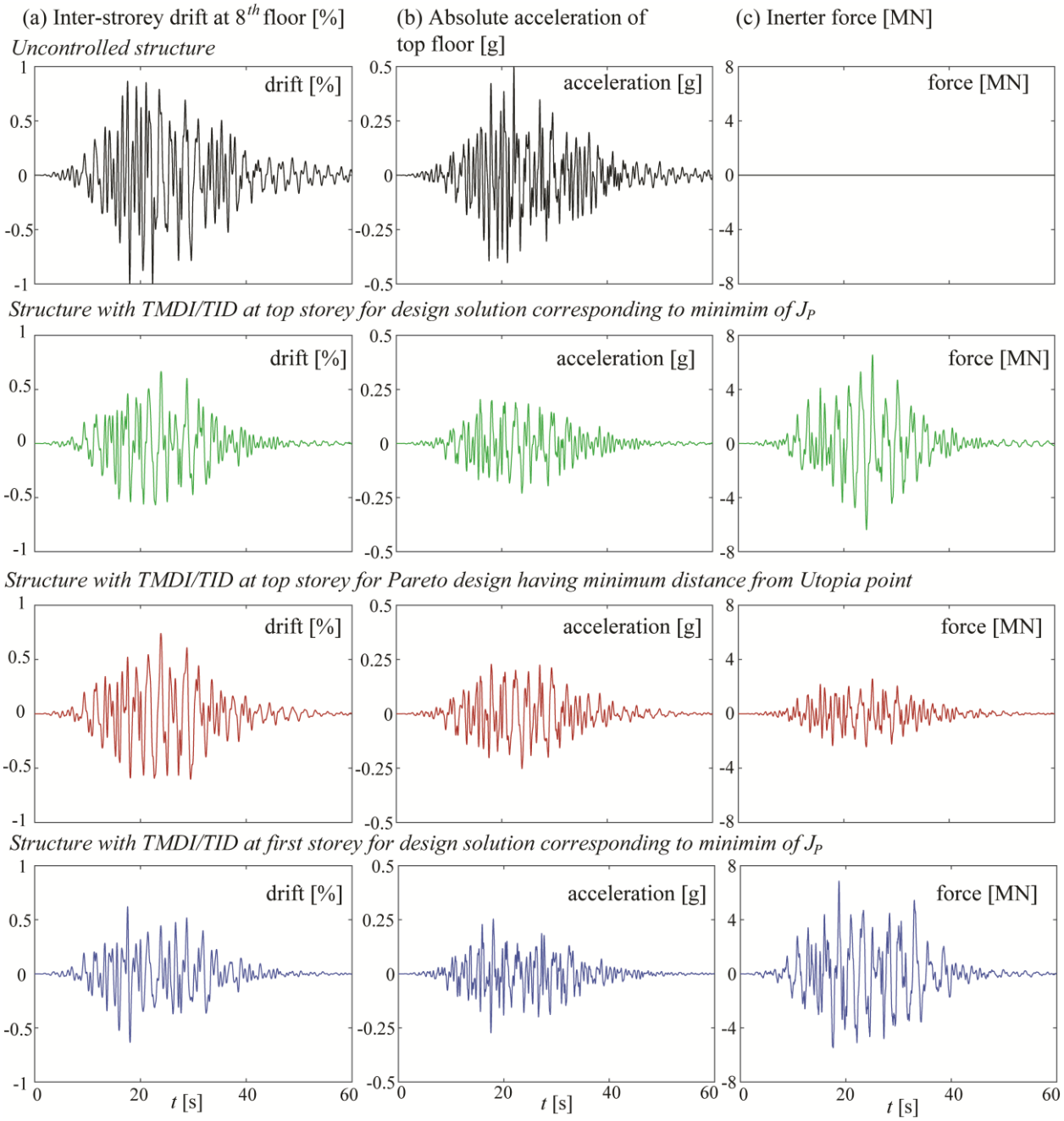

Figure 11: Response time-histories of uncontrolled benchmark building [top row] and controlled building with three different IVAs [second to fourth rows] under the non-stationary excitation shown in Figure 10(b). Time-histories correspond to: (a) drift of 8th story [first column], (b) absolute acceleration of top floor [second column] and (c) inerter force [third column].

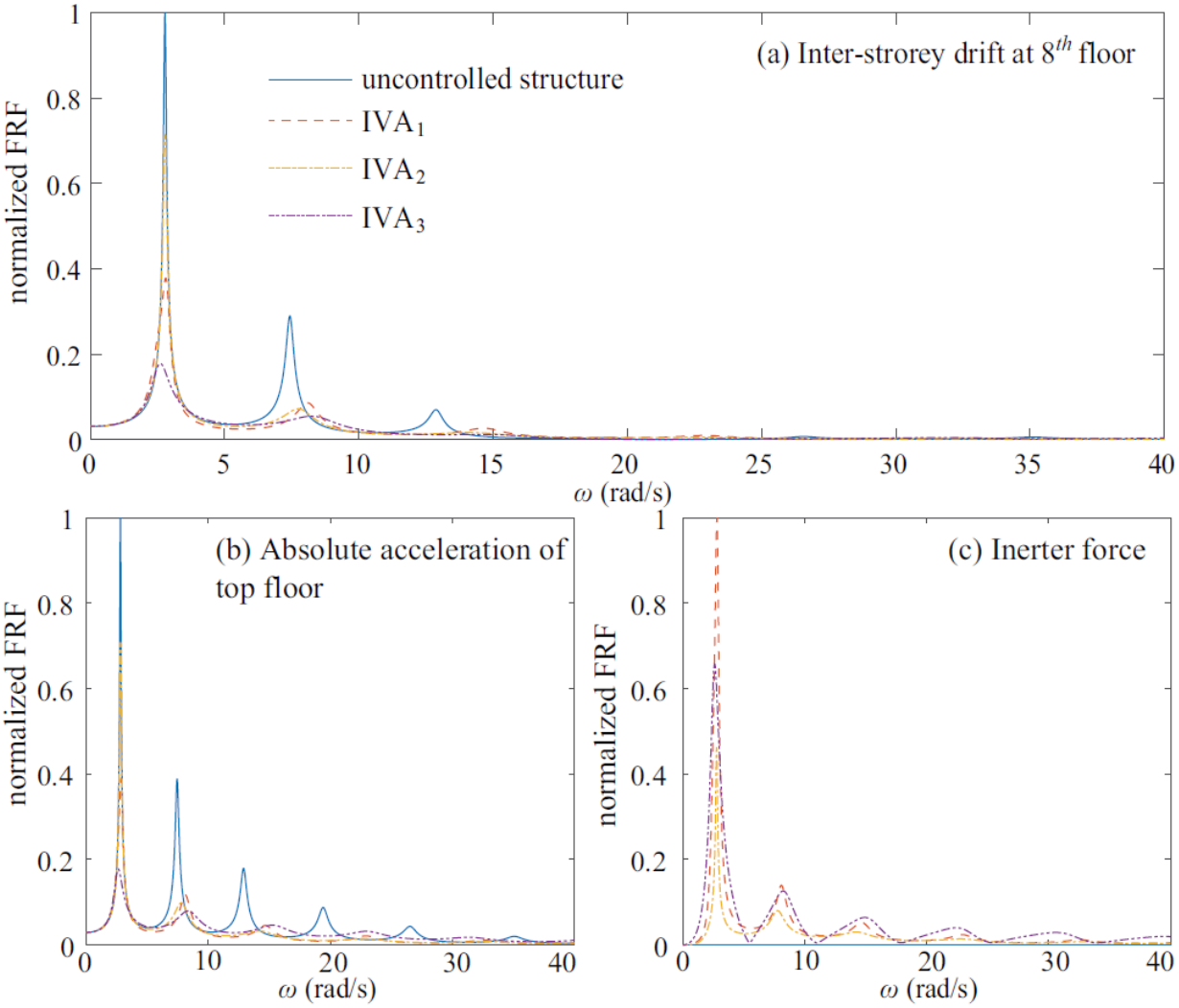

Figure 12: Normalized frequency response functions (FRFs) for the uncontrolled benchmark building and the three different IVA implementations shown in Figure 11. FRFs for the three different outputs shown in Figure 11 are shown.

Further insight for the performance of the implementations in Figure 11 is provided in Figure 12, showing the frequency response function (FRF), given by

$$H_{sz_i}(\omega\,|\,\boldsymbol{\varphi}) = \mathbf{n}_i^T \mathbf{C}_s(\boldsymbol{\varphi})[j\omega \mathbf{I}_{2(n+1)} - \mathbf{A}_s(\boldsymbol{\varphi})]^{-1} \mathbf{E}_s(\boldsymbol{\varphi}) \tag{25}$$

where $\mathbf{A}_s(\boldsymbol{\varphi})$, $\mathbf{E}_s(\boldsymbol{\varphi})$ and $\mathbf{C}_s(\boldsymbol{\varphi})$ are state-space matrices structure with IVA, described in Appendix A. The normalized FRF for the same three outputs (definition of z_i) as in Figure 11 are shown. Normalization is established so that peak value attained in each figure corresponds to 1. Therefore, FRFs for drift and acceleration are normalized with respect to the peak FRF value of the uncontrolled structure and FRF for forces are normalized with respect to peak FRF value of IVA_1 equipped structure. The FRF themselves follow same patterns observed in past studies [32] with introduction of the IVA influencing response across

a wide frequency range. FRF results across the IVAs demonstrate the same trends as observed in Figure 11, especially for the comparisons close to the fundamental system frequency. IVA_3 provides improvement compared to IVA_1 across all examined outputs, whereas IVA_2 offers compromise compared to IVA_1 with respect to vibration suppression (FRF for drift and acceleration) and IVA force (FRF for force).

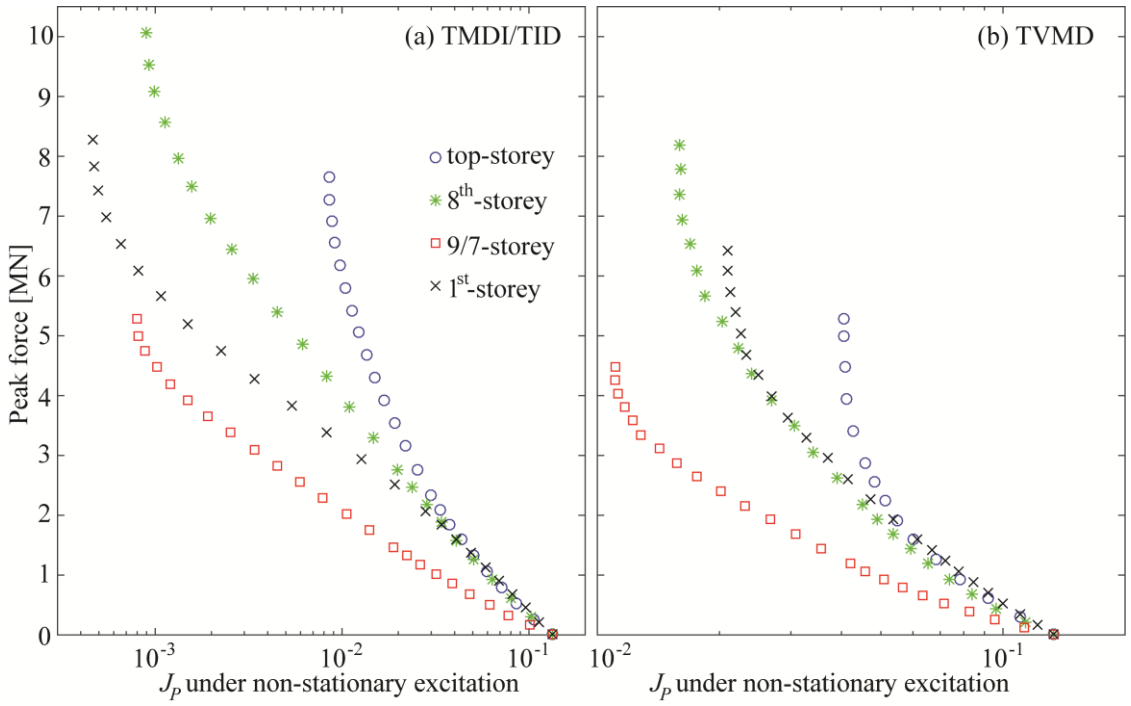

Figure 12: Performance under non-stationary excitation for balanced design application and for different placements for (a) TMDI/TID and (b) TVMD.

Whilst indicative, the deterministic performance verification of optimal IVAs designed under stationary excitation in Figure 11 is limited as it pertains to a single non-stationary excitation signal. To extend this assessment to a probabilistic context, an ensemble of 10^4 non-stationary ground motions is first generated using Eq.(24) and non-stationary response time-histories of the benchmark building equipped with IVAs optimally designed under stationary conditions are obtained through standard time-integration of Eq.(8) for the above generated ground motions. Next, ensemble response statistics are calculated to quantify structural performance under non-stationary conditions within a standard Monte Carlo simulation context. The metrics used for verifying performance for non-stationary conditions are consistent to the ones adopted at the IVA design stage under stationary excitation. Specifically, objective J_P in Eq. (15) is transformed to its equivalent expression, with probability $P_i(\boldsymbol{\varphi} \mid \beta_i, T)$ given by same expression in Eq. (12), with T substituted by the entire duration of the non-stationary excitation and z_i corresponding to the non-stationary response. Objective J_2 is replaced by the *peak IVA force*, given by the maximum force (in magnitude) developed

during the entire duration of the non-stationary excitation. Figures 12 and 13 show results for the non-stationary excitation, replicating Figures 4 and 9, respectively, with respect to non-stationary performance metrics. Trends are identical in all instances to the ones reported earlier for stationary conditions; performance has still characteristics of a Pareto front whereas comparison among different IVA placement (Figure 12) and design formulation (Figure 13) lead to same conclusions as for the stationary case. This is a practically important result, demonstrating that the stationary excitation/response assumption suffices to address typical amplitude non-stationary features exhibited by seismic ground motions. Indeed, even values for performance metrics are similar. The relationship between peak device force (non-stationary response) and standard deviation of that force (stationary response) is around 2-2.5, close to the expected peak factor value for the adopted illustrative building structure in which the relationship of strong ground motion duration to fundamental period is close to 7 [53]. On the other hand, the value of J_P is very similar for the two excitation conditions, especially for IVA designs corresponding to smaller J_P values (i.e., better vibration suppression). The better agreement for such IVA designs is justified by the fact that they endow the building with higher supplemental damping (hence the improved vibration suppression), for which non-stationary response statistics are expected to converge more rapidly to the stationary ones during the plateau of the excitation envelope [47].

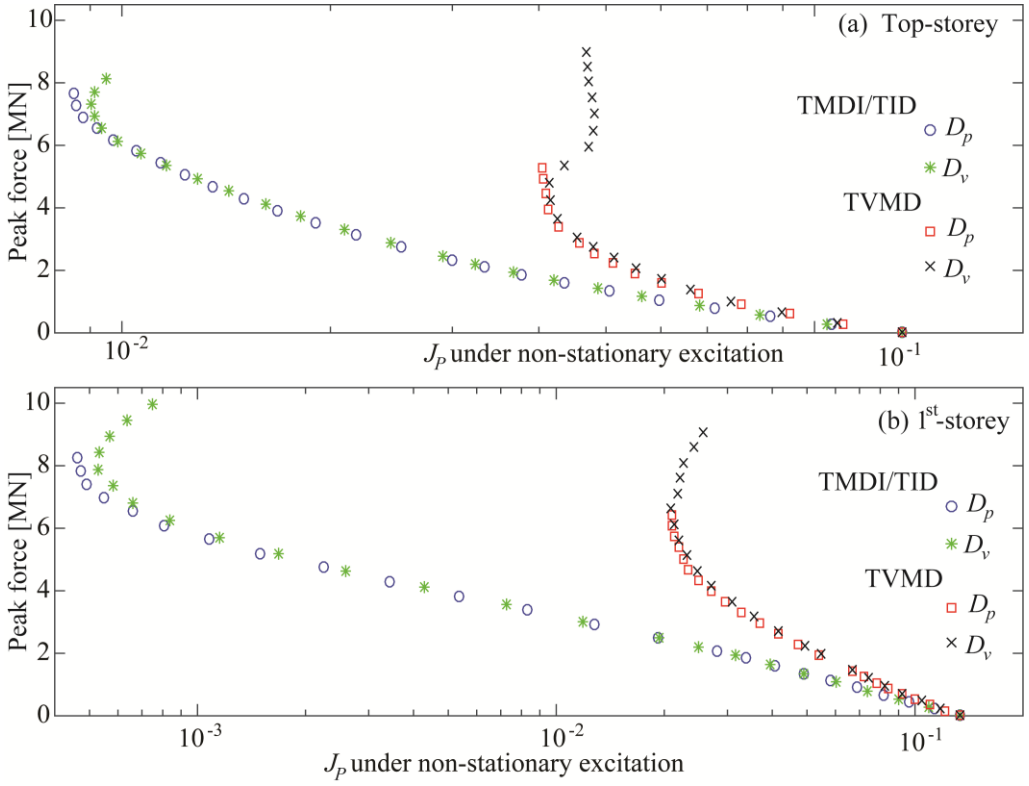

Figure 13: Comparison under non-stationary excitation of D_p and D_v formulations for balanced design application and IVA placement at (a) top-storey or (b) 1st-storey.

7. Concluding remarks

The efficiency of linear passive inerter-based vibration absorbers (IVAs) for seismic protection of multi-storey building structures has been examined under optimal design against two competing objectives: (i) suppressing building (host structure) earthquake-induced vibrations, and (ii) avoiding development of excessive IVA (control) forces exerted to the host structure. This was achieved by formulating a multi(bi)-objective optimal design problem and solving it via the epsilon-constraint approach to tune stiffness, damping, and inertia (inertance and/or mass) IVA properties given a linear host structure base-excited by stationary colored noise. The latter was defined in the illustrative case study by the filtered Kanai-Tajimi model widely-used in earthquake engineering to account for the frequency content of the seismic action to structures. One rigorous and one simpler optimal design formulations were considered with respect to the metric used to quantify objective (i), representing seismic performance of the host structure. The rigorous formulation quantified objective (i) through an equally weighted sum of probabilities that the engineering demand parameters (EDPs) of interest within a performance-based seismic design context (i.e., storey drifts and/or floor accelerations) exceed a pre-specified threshold. These probabilities were calculated semi-analytically through first-passage reliability criteria using the EDP out-crossing rates. The variant, simpler, formulation quantified structural performance (objective (i)) using equally weighted sum of EDP variances in accordance to traditional $\mathcal{H}_2$-style optimal tuning methods for mass dampers in stochastically excited structures. In both formulations, objective (ii) was quantified through the variance of the force transferred from the IVA to the host benchmark building.

In the numerical part of the paper, comprehensive optimal Pareto designs were furnished, obtained by both problem formulations, for the three best-established in the earthquake engineering literature IVAs, namely the tuned mass-damper-inerter (TMDI), the tuned inerter-damper (TID) and the tuned viscous-mass-damper (TVMD), and for various practically relevant IVA placements along the height of a benchmark (realistic) 9-storey steel building. Moreover, the efficacy of the above IVA designs optimized under stationary excitation and structural response conditions was verified for a non-stationary stochastic excitation model consistent with the stationary one in terms of duration and frequency content capturing typical evolutionary features of the amplitude of recorded earthquake accelerograms. The comparison between stationary and non-stationary performance was enabled by adopting equivalent with the stationary case metrics for quantifying objectives (i) and (ii) under non-stationary excitation/response conditions computed via standard Monte Carlo simulation. The overarching conclusions drawn from the numerical results presented are summarized as follows:

- The proposed multi-objective design approach can trace effectively the compromise between the two considered competing objectives (building performance in terms of storey drifts and

floor accelerations versus IVA control force exerted to the building), providing a range of Pareto optimal IVA designs to choose from.

- Considerable reduction of IVA control force transferred to the building of up to 3 times can be achieved with small deterioration of building performance compared to the extreme Pareto optimal IVA design targeting maximum building vibration suppression level.
- TID and TMDI achieve practically the same building performance and significantly outperform the TVMD, especially when targeting primarily floor acceleration mitigation (acceleration-sensitive design application adopting only floor accelerations as EDPs).
- Placement of IVAs at the ground (1st) storey improves performance across both objectives (i) and (ii) considered compared to placement at the top storey and even more so does IVAs spanning the two upper stories. This indicates that proper placement of the IVA device is an important consideration.
- The simplified design formulation minimizing the sum of EDP variances may provide significantly suboptimal performance compared to reliability-based performance criteria related to the probability of trespassing acceptable EDP thresholds which are better aligned with the modern performance-based seismic design framework.
- The assumption of stationary excitation/response conditions for IVA optimal design neither affects the quality of the converged Pareto optimal solutions nor the identified corresponding trends compared to non-stationary conditions and, therefore, stationary colored noise excitation models capturing local soil conditions suffice for effective IVA tuning for the seismic protection of building structures.

Appendix A: State-space formulation details

This appendix includes details about the formulation of the different state-space models discussed in this paper. Starting with the *n*-storey structure in Eqs. (3) and (4), its equivalent state-space description is

$$\begin{aligned}\dot{\mathbf{x}}_{ss}(t) &= \mathbf{A}_s(\boldsymbol{\varphi})\mathbf{x}_{ss}(t) + \mathbf{E}_s(\boldsymbol{\varphi})\ddot{x}_g(t)\\ \mathbf{z}(t) &= \mathbf{C}_s(\boldsymbol{\varphi})\mathbf{x}_{ss}(t),\end{aligned} \tag{A.1}$$

where $\mathbf{x}_{ss} \in \Re^{2n+2}$ is the state vector collecting relative to the ground displacements and velocities of all stories and of the spring/inerter connection point (relative to i_b floor), $\mathbf{x}_{ss} = [\mathbf{x}_s^T \quad y \quad \dot{\mathbf{x}}_s^T \quad \dot{y}]^T$, and the matrices in Eq. (A.1) are defined as

$$\mathbf{A}_s(\boldsymbol{\varphi})=\begin{bmatrix} \mathbf{0}_{(n+1)\text{x}(n+1)} & \mathbf{I}_{(n+1)} \\ -\mathbf{M}_t^{-1}(\boldsymbol{\varphi})\begin{bmatrix}\mathbf{K}_s & \mathbf{0}_{n\text{x}1}\\ \mathbf{0}_{1\text{x}n} & k_d\end{bmatrix} & -\mathbf{M}_t^{-1}(\boldsymbol{\varphi})\begin{bmatrix}\mathbf{C}_s & \mathbf{0}_{n\text{x}1}\\ \mathbf{0}_{1\text{x}n} & c_d\end{bmatrix}\end{bmatrix}$$

$$\mathbf{E}_s(\boldsymbol{\varphi})=\begin{bmatrix} \mathbf{0}_{(n+1)\text{x}1} \\ -\mathbf{M}_t^{-1}(\boldsymbol{\varphi})\begin{bmatrix}\mathbf{M}_s+\mathbf{R}_d m_d \mathbf{R}_d^T\\ m_d\mathbf{R}_d^T\end{bmatrix}\mathbf{R}_s\end{bmatrix} \tag{A.2}$$

$$\mathbf{C}_s(\boldsymbol{\varphi})=\begin{bmatrix} \mathbf{T}_s & \mathbf{0}_{n\text{x}(n+2)} \\ \begin{bmatrix}\mathbf{0}_{n\text{x}(n+1)} & \mathbf{I}_n & \mathbf{0}_{n\text{x}1}\end{bmatrix}\mathbf{A}_s(\boldsymbol{\varphi}) \\ b\begin{bmatrix}\mathbf{R}_c^T & 1\end{bmatrix}\begin{bmatrix}\mathbf{0}_{(n+1)\text{x}(n+1)} & \mathbf{I}_{n+1}\end{bmatrix}\mathbf{A}_s(\boldsymbol{\varphi})+c_d\begin{bmatrix}\mathbf{R}_c^T & 1\end{bmatrix}\begin{bmatrix}\mathbf{0}_{(n+1)\text{x}(n+1)} & \mathbf{I}_{n+1}\end{bmatrix} \\ c_d\begin{bmatrix}\mathbf{0}_{1\text{x}2n+1} & 1\end{bmatrix}+k_d\begin{bmatrix}\mathbf{0}_{1\text{x}n} & 1 & \mathbf{0}_{1\text{x}n+1}\end{bmatrix}\end{bmatrix}$$

In the above expressions, the output matrix $\mathbf{C}_s(\boldsymbol{\varphi})$ accounts for a performance (output) variables vector $\mathbf{z}$ that includes inter-storey drifts and absolute accelerations for all floors, and forces $f_b(t)$ and $f_d(t)$, respectively. Further, $\mathbf{I}_a$ is the identity matrix of dimension a, $\mathbf{0}_{axb}$ is the zero matrix of dimensions axb, $\mathbf{T}_s$ is a transformation matrix defining relative responses between consecutive floors (i.e., a square matrix with dimension n_s with 1 in the diagonal and -1 in the first off-diagonal), and the auxiliary matrix $\mathbf{M}_t(\boldsymbol{\varphi})$ reads as

$$\mathbf{M}_t(\boldsymbol{\varphi},\boldsymbol{\theta}_s)=\begin{bmatrix}\mathbf{M}_s(\boldsymbol{\theta}_s)+\mathbf{R}_d m_d\mathbf{R}_d^T+\mathbf{R}_c b\mathbf{R}_c^T & m_d\mathbf{R}_d+b\mathbf{R}_c\\ m_d\mathbf{R}_d^T+b\mathbf{R}_c^T & m_d+b\end{bmatrix}. \tag{A.3}$$

Combining Eqs. (A.1) and (7) leads to the representation in Eq. (8) where

$$\mathbf{x}=\begin{bmatrix}\mathbf{x}_{ss}\\ \mathbf{x}_q\end{bmatrix}\quad \mathbf{A}(\boldsymbol{\varphi})=\begin{bmatrix}\mathbf{A}_s(\boldsymbol{\varphi}) & \mathbf{E}_s(\boldsymbol{\varphi})\mathbf{C}_q\\ \mathbf{0}_{n_q\text{x}(2n+2)} & \mathbf{A}_q(\boldsymbol{\varphi})\end{bmatrix}\quad \mathbf{E}=\begin{bmatrix}\mathbf{0}_{2(n+1)\text{x}1}\\ \mathbf{E}_q\end{bmatrix}\quad \mathbf{C}(\boldsymbol{\varphi})=\begin{bmatrix}\mathbf{C}_s(\boldsymbol{\varphi}) & \mathbf{0}_{n_z\text{x}n_q}\end{bmatrix} \tag{A.4}$$

Lastly, the state-space matrices of the excitation model utilized in the illustrative example, leading to a stochastic process with spectral density given by Eq. (22), read as

$$\mathbf{A}_q=\begin{bmatrix}0 & 1 & 0 & 0\\ -\omega_g^2 & -2\zeta_g\omega_g & 0 & 0\\ 0 & 0 & 0 & 1\\ -\omega_g^2 & -2\zeta_g\omega_g & -\omega_f^2 & -2\zeta_f\omega_f\end{bmatrix}\quad \mathbf{E}_q=\begin{bmatrix}0\\1\\0\\0\end{bmatrix} \tag{A.5}$$

$$\mathbf{C}_q=\sqrt{2\pi s_o}\begin{bmatrix}-\omega_g^2 & -2\zeta_g\omega_g & \omega_f^2 & 2\zeta_f\omega_f\end{bmatrix}$$

Appendix B: Out-crossing rate calculation

This appendix discusses the estimation of the two different components of the out-crossing rate described in Eq.(13). Rice's unconditional outcrossing rate [50] is given by

$$r_i^+(\boldsymbol{\varphi}) = \frac{\sigma_{\dot{z}_i}(\boldsymbol{\varphi})}{\pi\sigma_{z_i}(\boldsymbol{\varphi})} \mathrm{e}^{-\frac{\beta_i^2}{2\sigma_{z_i}^2(\boldsymbol{\varphi})}} \tag{B.1}$$

where $\sigma_{\dot{z}_i}^2$ is the variance of $\dot{z}_i$ which is given by

$$\sigma_{\dot{z}_i}^2(\boldsymbol{\varphi}) = \mathbf{n}_i^T \mathbf{C}(\boldsymbol{\varphi})\mathbf{A}(\boldsymbol{\varphi})\mathbf{P}(\boldsymbol{\varphi})\mathbf{A}(\boldsymbol{\varphi})^T \mathbf{C}(\boldsymbol{\varphi})^T \mathbf{n}_i \tag{B.2}$$

assuming that the condition $\mathbf{C}(\boldsymbol{\varphi})\mathbf{E}(\boldsymbol{\varphi})=0$ holds. Note that this condition is necessary to ensure that the out-crossing rate of the z_i stochastic process is finite [46]. For the temporal correction factor, the one proposed by Taflanidis and Beck [49] is utilized here since it has been shown to provide good accuracy for dynamical systems with important higher order dynamics, as will be the case for multi-storey structures, especially when response outputs corresponding to structural acceleration are considered. This factor is given by:

$$\lambda_i(\boldsymbol{\varphi}) \approx \frac{1-\exp\left\{-q(\boldsymbol{\varphi})^{0.6}\left(\frac{2}{\sqrt{\pi}}\right)^{0.1}\frac{\beta_i\sqrt{2}}{\sigma_{z_i}(\boldsymbol{\varphi})}\right\}}{1-\exp\left\{-\frac{\beta_i^2}{2\sigma_{z_i}^2(\boldsymbol{\varphi})}\right\}};\ q(\boldsymbol{\varphi}) = \frac{\sigma_{z_i}^6(\boldsymbol{\varphi})}{4\pi\int_{-\infty}^{\infty}|\omega|S_{z_i z_i}(\omega\,|\,\boldsymbol{\varphi})d\omega\int_{-\infty}^{\infty}S_{z_i z_i}^2(\omega\,|\,\boldsymbol{\varphi})d\omega}, \tag{B.3}$$

where $S_{z_i z_i}(\omega\,|\,\boldsymbol{\varphi})$ is the spectral density function for z_i which can be calculated as

$$S_{z_i z_i}(\omega\,|\,\boldsymbol{\varphi}) = S_w\left|H_{z_i}(\omega\,|\,\boldsymbol{\varphi})\right|^2, \tag{B.4}$$

with $H_{z_i}(\omega\,|\,\boldsymbol{\varphi})$ corresponding to the frequency response function for z_i. Leveraging the state-space formulation of Eq. (8) the latter can be obtained as

$$H_{z_i}(\omega\,|\,\boldsymbol{\varphi}) = \mathbf{n}_i^T \mathbf{C}(\boldsymbol{\varphi})[j\omega\mathbf{I}_{n_x} - \mathbf{A}(\boldsymbol{\varphi})]^{-1}\mathbf{E}. \tag{B.5}$$

The two one-dimensional integrals in denominator of $q(\boldsymbol{\varphi})$ in Eq. (B.3) are calculated via standard numerical integration, using Eqs. (B.5) and (B.4) to estimate at each desired frequency ω the spectral density $S_{z_i z_i}(\omega\,|\,\boldsymbol{\varphi})$.

References

[1] I. Avramidis, A. Athanatopoulou, K. Morfidis, A. Sextos, A. Giaralis, Eurocode-Compliant Seismic Analysis and Design of R/C Buildings, Springer, 2015.
[2] C. Christopoulos, A. Filiatrault, Principles of passive supplemental damping and seismic isolation, IUSS Press, Pavia, Italy, 2006.
[3] D. Lee, D.P. Taylor, Viscous damper development and future trends, The Structural Design of Tall Buildings, 10 (5) (2001) 311-320.
[4] M.G. Soto, H. Adeli, Tuned mass dampers, Archives of Computational Methods in Engineering, 20 (4) (2013) 419-431.
[5] C.A. Goulet, C.B. Haselton, J. Mitrani-Reiser, J.L. Beck, G. Deierlein, K.A. Porter, J.P. Stewart, Evaluation of the seismic performance of code-conforming reinforced-concrete frame building-From

seismic hazard to collapse safety and economic losses, Earthquake Engineering and Structural Dynamics, 36 (13) (2007) 1973-1997.
[6] I.F. Lazar, S.A. Neild, D.J. Wagg, Using an inerter-based device for structural vibration suppression, Earthquake Engineering & Structural Dynamics, 43 (8) (2013) 1129-1147.
[7] K. Ikago, K. Saito, N. Inoue, Seismic control of single-degree-of-freedom structure using tuned viscous mass damper, Earthquake Engineering & Structural Dynamics, 41 (3) (2012) 453-474.
[8] K. Ikago, Y. Sugimura, K. Saito, N. Inoue, Modal response characteristics of a multiple-degree-of-freedom structure incorporated with tuned viscous mass dampers, Journal of Asian Architecture and Building Engineering, 11 (2) (2012) 375-382.
[9] L. Marian, A. Giaralis, Optimal design of a novel tuned mass-damper-inerter (TMDI) passive vibration control configuration for stochastically support-excited structural systems, Probabilistic Engineering Mechanics, 38 (2014) 156-164.
[10] A. Giaralis, L. Marian, Use of inerter devices for weight reduction of tuned mass-dampers for seismic protection of multi-story building: the Tuned Mass-Damper-Interter (TMDI), in: SPIE 9799, Active and Passive Smart Structures and Integrated Systems Las Vegas, Nevada, 2016, pp. doi:10.1117/1112.2219324.
[11] S.Y. Zhang, J.Z. Jiang, S. Neild, Optimal configurations for a linear vibration suppression device in a multi-storey building, Structural Control and Health Monitoring, 24 (3) (2017) e1887.
[12] S.Y. Zhang, J.Z. Jiang, S.A. Neild, Passive vibration control: a structure–immittance approach, Proc. R. Soc. A, 473 (2201) (2017) 20170011.
[13] K. Saito, Y. Sugimura, S. Nakaminami, H. Kida, N. Inoue, Vibration tests of 1-story response control system using inertial mass and optimized soft spring and viscous element, in: 14th World Conference on Earthquake Engineering, Beijing, China, 2008, pp. 12-01.
[14] J.-S. Hwang, J. Kim, Y.-M. Kim, Rotational inertia dampers with toggle bracing for vibration control of a building structure, Engineering Structures, 29 (6) (2007) 1201-1208.
[15] K. Ikago, Y. Sugimura, K. Saito, N. Inoue, Seismic displacement control of multiple-degree-of-freedom structures using tuned viscous mass dampers, in: 8th International Conference on Structural Dynamics, Leuven, Belgium., 2011, pp. 1800-1807.
[16] R.M. Hessabi, O. Mercan, Investigations of the application of gyro-mass dampers with various types of supplemental dampers for vibration control of building structures, Engineering Structures, 126 (2016) 174-186.
[17] L. Marian, A. Giaralis, Optimal design of inerter devices combined with TMDs for vibration control of buildings exposed to stochastic seismic excitations, in: 11th International Conference on Structural Safety and Reliability, New York, US, 2013, pp. 1025-1032.
[18] M.C. Smith, Synthesis of mechanical networks: the inerter, Automatic Control, IEEE Transactions on, 47 (10) (2002) 1648-1662.
[19] C. Papageorgiou, M.C. Smith, Laboratory experimental testing of inerters, in: Decision and Control, 2005 and 2005 European Control Conference. CDC-ECC'05. 44th IEEE Conference on, IEEE, 2005, pp. 3351-3356.
[20] L. Marian, A. Giaralis, The tuned mass-damper-inerter for harmonic vibrations suppression, attached mass reduction, and energy harvesting, Smart Structures and Systems, 19 (6) (2017) 665-678.
[21] S.J. Swift, M.C. Smith, A.R. Glover, C. Papageorgiou, B. Gartner, N.E. Houghton, Design and modelling of a fluid inerter, International Journal of Control, 86 (11) (2013) 2035-2051.
[22] X. Liu, J.Z. Jiang, B. Titurus, A. Harrison, Model identification methodology for fluid-based inerters, Mechanical Systems and Signal Processing, 106 (2018) 479-494.
[23] A. Gonzalez-Buelga, L. Clare, S. Neild, J. Jiang, D. Inman, An electromagnetic inerter-based vibration suppression device, Smart Materials and Structures, 24 (5) (2015) 055015.
[24] J.-Y. Li, S. Zhu, Versatile Behaviors of Electromagnetic Shunt Damper With a Negative Impedance Converter, IEEE/ASME Transactions on Mechatronics, 23 (3) (2018) 1415-1424.
[25] T. Arakaki, H. Kuroda, F. Arima, Y. Inoue, K. Baba, Development of seismic devices applied to ball screw: Part 1 Basic performance test of RD-series, AIJ Journal of Technology and Design, 8 (1999) 239-244 (in Japanese).
[26] H. Kuroda, F. Arima, K. Baba, Y. Inoue, Principles and characteristics of viscous damping devices (gyro-damper), the damping forces which are highly amplified by converting the axial movement to rotary one, in: 12th world conference on earthquake engineering, Oakland, New Zealand, 2000.

[27] Y. Sugimura, W. Goto, H. Tanizawa, K. Saito, T. Nimomiya, Response control effect of steel building structure using tuned viscous mass damper, in: 15th World Conference on Earthquake Engineering, Lisbon, Portugal, 2012.
[28] M. De Angelis, S. Perno, A. Reggio, Dynamic response and optimal design of structures with large mass ratio TMD, Earthquake Engineering & Structural Dynamics, 41 (1) (2012) 41-60.
[29] J.P. Den Hartog, Mechanical Vibrations, McGraw-Hill, Inc., New York, NY, 1947.
[30] S.F. Masri, J.P. Caffrey, H. Li, Transient Response of MDOF Systems With Inerters to Nonstationary Stochastic Excitation, Journal of Applied Mechanics, 84 (10) (2017) 101003.
[31] R.W. Clough, J. Penzien, Dynamics of structures, McGraw-Hill Inc., New York, N.Y, 1993.
[32] A. Giaralis, A.A. Taflanidis, Optimal tuned mass-damper-inerter (TMDI) design for seismically excited MDOF structures with model uncertainties based on reliability criteria, Structural Control and Health Monitoring, 25 (2) (2018) e2082.
[33] A. Giaralis, F. Petrini, Wind-induced vibration mitigation in tall buildings using the tuned mass-damper-inerter, Journal of Structural Engineering, 143 (9) (2017) 04017127.
[34] S. Krenk, J. Høgsberg, Tuned resonant mass or inerter-based absorbers: unified calibration with quasi-dynamic flexibility and inertia correction, Proceedings of the Royal Socociety A, 472 (2016) 20150718.
[35] C. Pan, R. Zhang, Design of structure with inerter system based on stochastic response mitigation ratio, Structural Control and Health Monitoring, 25 (6) (2018) e2169.
[36] C. Pan, R. Zhang, H. Luo, C. Li, H. Shen, Demand-based optimal design of oscillator with parallel-layout viscous inerter damper, Structural Control and Health Monitoring, 25 (1) (2018) e2051.
[37] D. Pietrosanti, M. De Angelis, M. Basili, Optimal design and performance evaluation of systems with Tuned Mass Damper Inerter (TMDI), Earthquake Engineering & Structural Dynamics, (2017).
[38] Y. Wen, Z. Chen, X. Hua, Design and Evaluation of Tuned Inerter-Based Dampers for the Seismic Control of MDOF Structures, Journal of Structural Engineering, 143 (4) (2016) 04016207.
[39] N. Makris, G. Kampas, Seismic protection of structures with supplemental rotational inertia, Journal of Engineering Mechanics, 142 (11) (2016) 04016089.
[40] F. Saitua, D. Lopez-Garcia, A.A. Taflanidis, Optimization of height-wise damper distributions considering practical design issues, Engineering Structures, 173 (2018) 768-786.
[41] Y. Ohtori, R. Christenson, B. Spencer Jr, S. Dyke, Benchmark control problems for seismically excited nonlinear buildings, Journal of Engineering Mechanics, 130 (4) (2004) 366-385.
[42] R.L. Keeney, H. Raiffa, Decisions with multiple Objectives: Preferences and Trade-offs, Cambridge University Press, 1993.
[43] L. Guenfaf, M. Djebiri, M. Boucherit, F. Boudjema, Generalized minimum variance control for buildings under seismic ground motion, Earthquake Engineering & Structural Dynamics, 30 (7) (2001) 945-960.
[44] M.P. Singh, L.M. Moreschi, Optimal placement of dampers for passive response control, Earthquake Engineering & Structural Dynamics, 31 (4) (2002) 955-976.
[45] S. Nagarajaiah, S. Narasimhan, Smart base isolated benchmark building. Part II - phase I sample controllers for linear isolation system., Journal of Structural Control and Health Monitoring, 13 (2-3) (2006) 589-604.
[46] A.A. Taflanidis, J.T. Scruggs, Performance measures and optimal design of linear structural systems under stochastic stationary excitation, Structural Safety, 32 (5) (2010) 305-315.
[47] L.D. Lutes, S. Sarkani, Stochastic analysis of structural and mechanical vibrations, Prentice Hall, Upper Saddle River, NJ, 1997.
[48] K.A. Porter, A.S. Kiremidjian, J.S. LeGrue, Assembly-based vulnerability of buildings and its use in performance evaluation, Earthquake Spectra, 18 (2) (2001) 291-312.
[49] A.A. Taflanidis, J.L. Beck, Analytical approximation for stationary reliability of certain and uncertain linear dynamic systems with higher dimensional output, Earthquake Engineering and Structural Dynamics, 35 (10) (2006) 1247-1267.
[50] S.O. Rice, Mathematical analysis of random noise, Bell System Technical Journal, 23 and 24 (1944, 1945).
[51] K.A. Porter, R.P. Kennedy, R.E. Bachman, Creating fragility functions for performance-based earthquake engineering, Earthquake Spectra, 23 (2) (2007) 471-489.
[52] P. Dorato, C. Abdallah, V. Cerone, Linear-quadratic control: An introduction, Prentice Hall, 1998.

[53] A. Der Kiureghian, Structural response to stationary excitation, Journal of Engineering Mechanics, ASCE, 106 ((EM6)) (1980) 1195-1213.
[54] I. Gidaris, A.A. Taflanidis, Performance assessment and optimization of fluid viscous dampers through life-cycle cost criteria and comparison to alternative design approaches, Bulletin of Earthquake Engineering, 13 (4) (2015) 1003-1028.
[55] E. Zitzler, K. Deb, L. Thiele, Comparison of multiobjective evolutionary algorithms: Empirical results, Evolutionary computation, 8 (2) (2000) 173-195.
[56] Y.Y. Haimes, L. Ladson, D.A. Wismer, Bicriterion formulation of problems of integrated system identification and system optimization, IEEE Transactions on Systems Man and Cybernetics, (3) (1971) 296-&.
[57] K. Holmstrom, A.O. Goran, M.M. Edvall, User's guide for TOMLAB 7, Tomlab Optimization Inc. www.tomopt.com/tomlab/, San Diego, CA, 2010.
[58] J.D. Marshall, F.A. Charney, Seismic response of steel frame structures with hybrid passive control systems, Earthquake Engineering & Structural Dynamics, 41 (4) (2012) 715-733.
[59] G. Cimellaro, T. Soong, A. Reinhorn, Integrated design of controlled linear structural systems, Journal of Structural Engineering, 135 (7) (2009) 853-862.
[60] R.E. Steuer, Multiple criteria optimization: theory, computation, and application, 1989.
[61] D.M. Boore, Simulation of ground motion using the stochastic method, Pure and Applied Geophysics, 160 (2003) 635-676.
[62] A. Giaralis, P.D. Spanos, Derivation of response spectrum compatible non-stationary stochastic processes relying on Monte Carlo-based peak factor estimation, Earthquakes and Structures, 3 (3) (2012) 581-609.
[63] G. Housner, P.C. Jennings, Generation of artificial earthquakes, Journal of the Engineering Mechanics Division, 90 (1) (1964) 113-152.